REVIEW

National Science Review
4: 810–833, 2017
doi: 10.1093/nsr/nwx117
Advance access publication 22 September 2017

[1]State Key Laboratory of Earth Surface Processes and Resource Ecology, GCESS, Beijing Normal University, Beijing 1000875, China; [2]Department of Atmospheric and Oceanic Sciences, University of Maryland, MD 21029, USA; [3]State Key Laboratory of Severe Weather, Chinese Academy of Meteorological Sciences, Beijing 100081, China; [4]School of Atmospheric Sciences, Nanjing University, Nanjing 210023, China; [5]School of Environmental Science and Engineering, Nanjing University of Information Science and Technology, Nanjing 210044, China; [6]State Key Laboratory of Atmospheric Boundary Layer Physics and Atmospheric Chemistry, Institute of Atmospheric Physics, Chinese Academy of Sciences, Beijing 100029, China; [7]Center for Excellence in Regional Atmospheric Environment, Institute of Urban Environment, Chinese Academy of Sciences, Xiamen 361021, China; [8]Department of Atmospheric and Oceanic Sciences, Peking University, Beijing 100871, China and [9]School of Atmospheric Physics, Nanjing University of Information Science and Technology, Nanjing 210044, China

*Corresponding authors. E-mails: zhanqing@umd.edu; jpguocams@gmail.com

**Received** 30 March 2017; **Revised** 18 July 2017; **Accepted** 16 September 2017

ENVIRONMENT/ECOLOGY

Special Topic: Air Pollution and Control

# Aerosol and boundary-layer interactions and impact on air quality

Zhanqing Li[1,2,*], Jianping Guo[3,*], Aijun Ding[4], Hong Liao[5], Jianjun Liu[2], Yele Sun[6,7], Tijian Wang[4], Huiwen Xue[8], Hongsheng Zhang[8] and Bin Zhu[9]

## ABSTRACT

Air quality is concerned with pollutants in both the gas phase and solid or liquid phases. The latter are referred to as aerosols, which are multifaceted agents affecting air quality, weather and climate through many mechanisms. Unlike gas pollutants, aerosols interact strongly with meteorological variables with the strongest interactions taking place in the planetary boundary layer (PBL). The PBL hosting the bulk of aerosols in the lower atmosphere is affected by aerosol radiative effects. Both aerosol scattering and absorption reduce the amount of solar radiation reaching the ground and thus reduce the sensible heat fluxes that drive the diurnal evolution of the PBL. Moreover, aerosols can increase atmospheric stability by inducing a temperature inversion as a result of both scattering and absorption of solar radiation, which suppresses dispersion of pollutants and leads to further increases in aerosol concentration in the lower PBL. Such positive feedback is especially strong during severe pollution events. Knowledge of the PBL is thus crucial for understanding the interactions between air pollution and meteorology. A key question is how the diurnal evolution of the PBL interacts with aerosols, especially in vertical directions, and affects air quality. We review the major advances in aerosol measurements, PBL processes and their interactions with each other through complex feedback mechanisms, and highlight the priorities for future studies.

**Keywords:** aerosol, PBL, radiation, aerosol–PBL interaction, climate change

## INTRODUCTION

Aerosols are multi-facet agents that affect air quality, weather and climate through many mechanisms, as reviewed extensively in a series of IPCC reports. Aerosols are colloids of fine solid particles or liquid droplets suspended in the atmosphere. Through the effects of aerosol–radiation interactions (ARI), aerosol–cloud interactions (ACI) or both, aerosols can significantly affect Earth's climate by perturbing the Earth's radiation budget and water cycle processes [1–8]. As some observational analyses have indicated, cloud and precipitation properties are remarkably affected by elevated aerosols, which suppress light rainfall but intensify heavy rainfall and lightning in the coastal regions of Southeast China [9]. Aerosol pollution in the planetary boundary layer (PBL) adversely affects human health [10,11]. Chemical reactions can occur on the surface of non-gaseous particles or within the body of liquid droplets, and these processes are key components of the biogeochemistry of our planet [12].

The ARI effect is concerned with the scattering and absorption of solar radiation by aerosol particles. Aerosols can substantially reduce the amount of solar radiation reaching the ground [13,14], and thus reduce sensible heat fluxes that drive the diurnal evolution of temperature and the PBL [15]. This in turn leads to weaker turbulence in the PBL, and a reduction of entrainment of dry air into the PBL from the free troposphere, which leads to more moisture in the PBL. The combined effects of lowering near-surface temperature and increased moisture can increase relative humidity (RH). The increased RH tends to favor the hygroscopic growth of aerosols and enhances the scattering of solar radiation. The

increased RH could also enhance the formation of secondary aerosols. The aqueous-phase reactions of $NO_2$ and $SO_2$ in fog/clouds or aerosol water are important for sulfate formation under hazy conditions in China [16–18].

It has been found that the discrepancy in aerosol types leads to huge differences in estimates of aerosol direct forcing at the top and bottom of the atmosphere over the Indian Ocean [14] and in China [19]. Also, it is well recognized that various aerosol types exhibit quite different ARI effects. Among all types of aerosols, absorbing aerosols, consisting primarily of organic carbon, black carbon (BC) and brown carbon [21], have the strongest interaction with the PBL [22]. In a polluted environment, BC can be transformed into fully compact particles and becomes a much stronger absorbing agent [23,24]. As such, absorbing aerosols can alter the PBL more effectively than other types of aerosol, which may be another major factor on top of the formation of new particles in triggering severe haze events in China [25].

The PBL is inherently connected to air pollution because of the bulk of aerosols residing in the PBL, and the strong interactions or feedbacks between aerosols and the PBL [26]. These interactions can considerably exacerbate air pollution, even if emission rates remain the same. Observational and modeling studies suggest that aerosol–PBL feedbacks influence air quality significantly. Surface dimming (by all types of aerosols) and upper-PBL warming (by absorbing aerosols) help stabilize the PBL and weaken turbulence mixing, leading to a decrease in the boundary-layer height (BLH), which correctively favors the accumulation of air pollutants in a shallower PBL [15,24,27].

The absorption of solar radiation by aerosols can induce a temperature inversion (TI) at the top of the PBL that is often associated with severe pollution episodes [28]. When the temperature difference between the top and bottom of a TI layer is greater than 20°F, severe pollution ensues [29]. Some of the most severe pollution events in history have been associated with elevated TIs. In general, high aerosol concentrations tend to occur in the atmosphere with a TI [30–32]. Gas pollutants such as $SO_2$ [33] and $NO_2$ [32,34] have also been found to be closely linked to TIs.

In this article, we comprehensively review the studies with regard to aerosol, pollution, PBL and their interactions, starting with the section entitled 'Overview of air pollution and aerosols in China'. PBL processes and observations are given in the section entitled 'Fundamentals and observations of the PBL'. Aerosol–PBL–convection interaction schemes are described in the section entitled 'Processes governing aerosol and PBL interactions'. The section entitled 'The trend and fluctuation of air pollution: the roles of circulation, PBL, climate change and weather' elaborates on the general roles of PBL, climate changes and weather regimes on surface air pollution. The section entitled 'Concluding remarks' concludes the paper.

## OVERVIEW OF AIR POLLUTION AND AEROSOLS IN CHINA

### Ground surface measurements

Aerosols have been measured extensively across China, chiefly after 2000, through national operational networks and field experiments, which have been comprehensively reviewed by Liao *et al.* [6] and Li *et al.* [7]. Prior to 2000, a few direct aerosol optical depth (AOD) measurements were made, which were inferred from clear-sky radiation data [35,36,], revealing a rapid deterioration of air quality from the 1960s to the 1990s. This was confirmed by concomitant satellite-derived AOD observations [37]. More accurate AOD measurements can be provided by ground-based sunphotometers. After 2000, several ground-based aerosol observation networks were established across China, including the Chinese Sun Hazemeter Network [38], the China Atmosphere Watch Network (CAWNET) [39], the China Aerosol Remote Sensing Network [40,41], and the Campaign on Atmospheric Aerosol Research network of China (CARE-China) by the Chinese Academy of Sciences [42]. Intensive field experiments measuring rich aerosol properties have been increasingly conducted in China, such as the East Asian Study of Tropospheric Aerosols: an International Regional Experiment (EAST-AIRE) [43] and the East Asian Study of Tropospheric Aerosols and Impact on Regional Climate [44].

These data have been widely used to derive the nationwide distribution of AOD [38] and aerosol single scattering albedo (SSA) [45]. Aerosol loading is exceptionally heavy in the eastern half of China. Aerosol absorption is particularly strong in central-west China and Northeast China due to the high consumption of coal (Shanxi is the capital of coal mining in China). There is much weaker absorption in southeastern China due presumably to its industrial emissions containing high proportions of sulfate and nitrate whose absorption is weak. Combining ground- and satellite-based measurements, Li *et al.* [20] for the first time derived the estimate of aerosol radiative forcing at the top, bottom, and within the atmosphere. The daily and annual mean atmospheric absorption and surface cooling due to aerosols

(primarily in the PBL) are $-20$ W m$^{-2}$ and 18 W m$^{-2}$, respectively.

Air pollution typically characterized by high concentration of aerosol particles in aerodynamic diameter less than 2.5 $\mu$m ($PM_{2.5}$) concentrations is one of the major environmental concerns in China. Although air quality in megacities has continued to improve since 2013, the annual mean $PM_{2.5}$ concentration in most cities in northern China is still much higher than the National Ambient Air Quality Standard (i.e. 35 $\mu$g m$^{-3}$ as an annual average), e.g. 70.3 $\mu$g m$^{-3}$ in Beijing in 2016. These results clearly indicate that air pollution in megacities in China is still severe, and it is even worse during the winter season because of the increased emissions by coal combustion for residential heating along with the frequent stagnant meteorological conditions. As a result, extensive ground measurements have been conducted during the past decade to characterize the chemical composition, sources and formation mechanisms of aerosol particles, with most of them taking place in the four most polluted regions, including the Pearl River Delta, the Yangtze River Delta, the North China Plain and the Sichuan Basin. This includes several international field campaigns by involving tens of research teams around the world, such as the Campaigns of Air Quality Research in Beijing and Surrounding Regions (CAREBeijing), the Program of Regional Integrated Experiments of Air Quality over Pearl River Delta (PRIDE-PRD) [39], and the Haze Observation Project Especially for Jing-Jin-Ji Area (HOPE $J^3A$) [46].

Numerous results and findings on aerosol composition, sources and processes have been presented. Overall, organic aerosols account for the major fraction of $PM_{2.5}$ followed by ammonium sulfate or ammonium nitrate, and black carbon. While the sources of primary emissions including traffic, coal combustion, biomass burning and cooking are identified and quantified, secondary aerosols are found to be more important in the formation of severe haze episodes [16,47,48]. It has been well recognized that the high anthropogenic emissions and rapid secondary aerosol formation are the key factors leading to the frequent occurrence of severe haze episodes, characterized by efficient new particle formation and growth [49]. The efficient aerosol nucleation, combined with aerosol growth, is closely associated with severe haze episodes in China. It is quite distinct from those typically observed in the urban regions of other countries and pristine environments worldwide [50], which are modulated by interactions between sulfuric acid and organics [51–54]. Typically, there exist clear diurnal variations in the PM number, size and mass concentration [55], reflecting the interplay between primary emissions, new particle formation, photochemical growth, removal and the PBL variation. In contrast, haze events in China typically exhibit a periodic cycle of 4–7 days [56].

In addition, recent studies have also illustrated the important roles of stagnant meteorology, which are typically characterized by low BLH, weak wind speed, strong temperature inversion and high RH in the formation of these events [57,58]. In fact, the favorable weather conditions induced by the increases in greenhouse gas emissions or the changes in the boreal cryosphere, particularly in the global environment, are mainly responsible for the more frequent haze episodes in winter on the North China Plain [59,60]. The most recent results from air pollution studies in China are summarized in [61], and the extensive ground measurements of aerosol particles based on real-time techniques are presented in [62].

## Aerosol vertical distributions and the PBL

The aerosol vertical distribution is key in determining aerosol radiative forcing. To date, our understanding of aerosol radiative forcing is still very poor due to the assumption of vertically constant profiles in radiative-transfer models, among other factors. Aerosol radiative forcing strongly depends on the vertical distribution of aerosols relative to clouds, especially for dust layers [63].

Using aircraft observations over the Beijing–Tianjin–Hebei region of North China, different types of aerosol vertical distributions in association with the PBL evolution have been revealed [64–66]. When the PBL is well developed, the aerosol number concentration ($N_a$) is homogeneously distributed throughout the whole PBL, leading to a sharp drop above the PBL top [66]. The vertical profile of aerosol number concentration ($N_a$) can then be approximated by a piecewise function [64].

Our understanding of the aerosol vertical structure has been improved tremendously since the advent of the Cloud–Aerosol Lidar with Orthogonal Polarization (CALIOP) onboard the Cloud–Aerosol Lidar and Infrared Pathfinder Satellite Observations satellite, which has become increasingly recognized as a valuable sensor to elucidate the altitude-resolved structure of aerosol particles such as smoke, dust and polluted dust [67]. While ground-based lidar and aircraft-borne *in situ* measurements have provided major insights into regional aerosol structure, CALIOP-based observations have been extensively used to derive the 3D structure of aerosols on a global scale [68]. By defining the most probable height (MPH) where aerosol particles most likely reside, Huang *et al.* [69] generated a global MPH distribution for dust and smoke aerosol types.

On regional scales, large discrepancies and uncertainties remain when it comes to the vertical distribution of aerosols at altitudes within the PBL up to the bottom of the free troposphere [70], depending on the regions and seasons of interest [71–74]. Specifically, Adams *et al.* [75] presented the 3D structure of aerosols across the trans-Atlantic region. Based on 10 dust cases observed by the CALIOP, Huang *et al.* [76] found that summertime dust storms occurred more frequently than previously thought on the remote northwestern Tibet Plateau, and that the dust layer reached altitudes of up to 4–7 km. Based on CALIOP observations, along with surface meteorological data and the Hybrid Single Particle Lagrangian Integrated Trajectory Model (HYSPLIT), Guo *et al.* [77] found that dust storms originating in northwestern China were transported eastward to Beijing at a rate of 1200 km per day, mostly at altitudes of 3–5 km. As shown in Fig 1, two zonal transport pathways were revealed from synergetic observations made by the CALIOP and the Moderate Resolution Imaging Spectroradiometer (MODIS): one dust belt across northern China and a smoke belt across southern China [78]. Recently, based on long-term satellite- and ground-based measurements, both seasonal and spatial variations of the profiles of aerosol extinction coefficients over China have been identified. In particular, the lapse rates of aerosol extinction in the polluted regions were much greater than those in the pristine regions, most likely due to more stable atmosphere caused by absorptive aerosols in the polluted regions [79].

The aerosol vertical distribution in the PBL, subject to the PBL dynamics and large-scale weather systems, exhibits strong temporal (seasonal and diurnal) variations and spatial differences, as revealed in the meteorological tower measurements of $PM_{2.5}$ and $PM_{10}$ in Beijing in 2003 [80]. Further subsequent measurements were made on the same tower to characterize the vertical distributions of trace gases (e.g. ozone ($O_3$), nitrogen dioxide ($NO_2$), and sulfur dioxide ($SO_2$)), $PM_{2.5}$ and filter-based aerosol composition [81–84]. The results showed that the mixing ratio of $O_3$ often peaked at ∼120 m and remained high in the residual layer at nighttime [85], while $SO_2$ was found to have the highest mixing ratio at ∼50 m [82]. More recently, Sun *et al.* [86,87] conducted simultaneous real-time observations of aerosol particle composition at two different heights on a tower, i.e. ground level and 260 m above ground level (AGL), using two similar aerosol mass spectrometers. The results illustrated very complex vertical distributions of aerosol species that interact closely with boundary-layer meteorology. In general, the vertical differences between ground level and 260 m AGL are reduced substantially in the daytime due to the elevated BLH associated with stronger vertical mixing. They also observed the interactions of different air masses at different heights that affect the vertical gradients. For example, the temperature inversion during the clearing stage of a severe pollution event results in a delay of the cleaning of air pollutants between ground level and 260 m AGL, while the stably stratified layer associated with a fog event is often characterized by much higher concentrations of aerosol species in the lower atmosphere and rapid decreases on the top of the layer. Further analysis shows that the vertical differences in meteorology (e.g. T and RH) and gas precursors can also affect secondary aerosol formation at different heights. For example, higher concentrations of nitrate at higher altitudes were clearly associated with

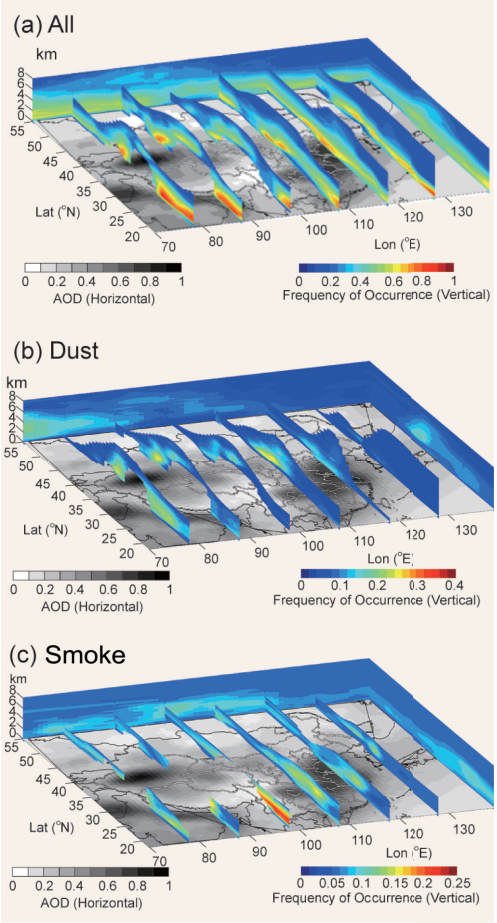


**Figure 1.** Annual mean 3D occurrence (color shaded) for (a) all aerosol types, (b) dust aerosols and (c) smoke aerosols, which are derived from level-2 CALIOP aerosol layer products, in combination with MODIS/Aqua AOD data (white–black shaded) for the period October 2006–September 2014. Note that only those with frequency greater than 5% are shown here. (Adapted from [78].)

the lower T and higher RH that facilitated the gas-to-particle formation mechanisms.

Although the vertical distributions of air pollution and its interaction with the boundary layer in the low atmosphere have been extensively characterized based on the tower measurements, our understanding of these characteristics and interactions at high altitude is far from complete. The vertical distribution of aerosol number concentration in the PBL over Beijing has been found to be strongly related to different weather systems, based on *in situ* aircraft measurements [66]. Distinct vertical profiles of aerosol scattering coefficient and precursors were found over cities in eastern, northwestern, and northeastern China [88]. Similar vertical distribution characteristics of aerosol optical properties were reported based on micropulse lidar data from the Yangtze River Delta of China [89]. Multi-layer BC in the PBL, including local accumulation near the surface and regional transport from upwind megacities in the upper PBL, was revealed using a tethered balloon platform [90]. In 2014, the vertical profiles of $O_3$ and size-resolved aerosol number concentrations were measured at a rural site on the North China Plain using an unmanned aerial vehicle [91]. The results showed higher $O_3$ levels in the residual layer than the mixed layer, while this is reversed for aerosol number concentrations. Further analysis illustrated that the vertical profiles of air pollutants are influenced by not only PBL meteorology, but also anthropogenic emissions on local and regional scales.

## FUNDAMENTALS AND OBSERVATIONS OF THE PBL

### PBL processes

A comprehensive review of the theory, nature and modeling of PBL was given in Baklanov *et al.* [92]. The physical processes in the PBL are concerned with turbulent diffusion, wind speed, the atmospheric thermodynamic state (i.e. temperature, humidity), and adiabatic heating due to aerosols and other absorbing agents. The wind and temperature profiles along with the BLH are the main factors affecting turbulent diffusion [81]. The PBL structure is also dictated by large-scale weather regimes [93].

Based on the Monin–Obukhov similarity theory of continuous turbulent motion, the relationship between flux (e.g. momentum, sensible and latent heat fluxes) and atmospheric profile (e.g. wind, humidity, temperature, gradient) in the atmospheric surface layer is key for air pollution diffusion, especially under stable stratification conditions. The structure of a stable boundary layer remains a puzzle in the PBL study. A series of experiments to tackle this issue have been carried out, such as the Stable Atmospheric Boundary-Layer Experiment in Spain [94], the Cooperative Atmospheric–Surface Exchange Study in Kansas [95], and the Surface Heat Budget of the Arctic Ocean Experiment in the Antarctic [96]. Turbulent intermittency frequently occurs in a stable boundary layer, which tends to scale up the transport of heat, water vapor, and momentum in the vertical, as opposed to the reduced vertical transport in the unstable boundary layer characterized by continuous turbulent motion [97]. The characteristics of such scalar quantities as $PM_{2.5}$ and $NO_x$ are affected by the turbulent velocity field and present a complex, chaotic structure on spatiotemporal scales, which makes it difficult to study the turbulent transport of pollutants [98]. The Hilbert–Huang transform method [99] is a valid method to solve atmospheric turbulence problems in a stable boundary layer and has been widely applied [100,101]. Currently, most topics associated with generalized PBL parameterization schemes in models are related to a stable boundary layer. For example, a systematic overestimation of simulated near-surface wind velocities under stable atmospheric conditions has been reported in addition to an overestimated turbulent diffusion capacity of air pollutants in a stable layer, resulting in the underestimation of pollution [102,103]. It is therefore imperative to explore and understand the structure of the stable boundary layer and its interaction with and influence on the air pollutant transport process.

### Detection and variations of BLH

Knowledge of the PBL is crucial for understanding the interactions between air pollution and meteorology. A key question remaining unclear is how the diurnal evolution of the PBL interacts with the vertical distributions of aerosols. To address this question, we need to have a good knowledge of the BLH and its evolution. The determination of BLH is a nontrivial task because it is not directly measured by routine meteorological instruments. The most common PBL observations are obtained by radiosondes, which can provide vertical temperature, moisture and wind profiles from the surface up to the ∼50-hPa level [104–106]. Various algorithms have been developed to retrieve the BLH; these have been completely summarized in Seidel *et al.* [107].

Guo *et al.* [108] obtained the first BLH climatology in China using long-term fine-resolution (1-s resolution) atmospheric soundings from the radiosonde observation network operated by the China Meteorological Administration. In addition to the spatial and seasonal variability of the BLH,

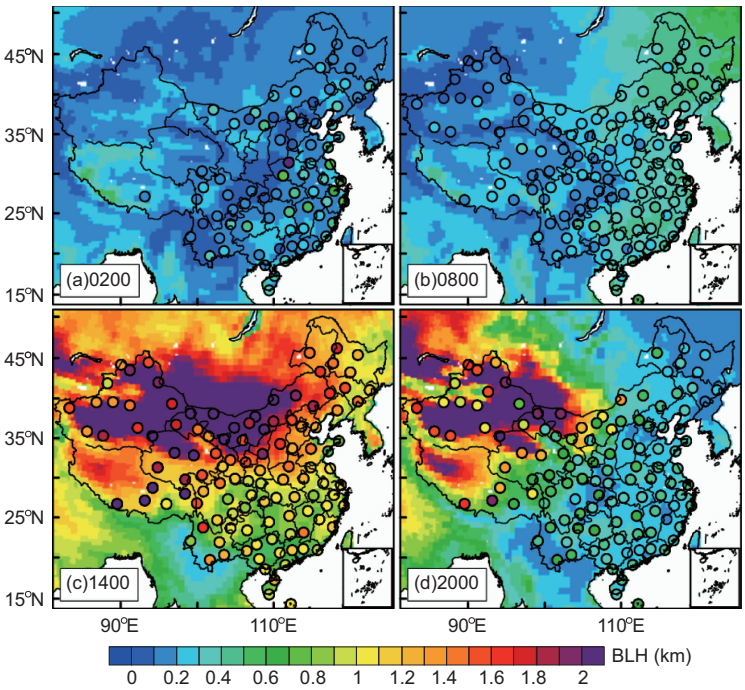


**Figure 2.** Spatial distribution of mean BLHs derived from summertime sounding measurements at (a) 0200, (b) 0800, (c) 1400 and (d) 2000 Beijing time in summers of the period 2011 to 2015 throughout the L-band China Radiosonde Network as operated by the China Meteorological Administration (colored dots), overlaid with those derived from simultaneous ERA-Interim reanalyses (color shading). (Adapted from [108].)

the diurnal cycles of PBL were investigated for the first time across China (Fig 2). A large discrepancy between sounding- and reanalysis-derived BLH was found, particularly in North China at 1400 Beijing time. This may undermine our ability to observe and simulate surface $PM_{2.5}$ because the latter relies on reanalysis-derived BLH data [40,109–111].

Although radiosondes are widely deployed around the world, operational radiosonde launches are done only twice a day (0000 UTC and 1200 UTC), prohibiting observation of the diurnal variation of the BLH. To overcome this limitation, various types of measurements have been used to derive the BLH, including more frequent launches of radiosondes that usually happen during a field experiment, ground-based remote sensing using high-resolution infrared sounder, multi-channel microwave radiometer, lidar, sodar, etc.

Among the various observation techniques, the lidar measurements have been most widely used to retrieve the PBL. The wavelet covariance transform method is one of the widely used algorithms; this is detailed by Davis *et al.* [112] and Brooks [113]. The algorithm allows for comparisons between the backscatter sounding and a step function, such that the largest gradient in backscatter with altitude is marked as the top of the PBL. The wavelet covariance transform is suitable for the automatic detection of the PBL because it requires only the lidar backscatter information. However, the wavelet covariance transform method often detects cloud backscatter and elevated aerosol plumes instead. To avoid this problem, Steyn *et al.* [114] fit the entire backscatter profile to an idealized curve. The algorithm uses an iterative curve-fitting routine to minimize the root-mean-square difference between the backscatter profile and the idealized curve. Simulated annealing allows the iterative process to bypass local solutions and returns a more robust BLH [115]. It also introduces a small random element that must be filtered out to avoid occasional unrealistic jumps in BLH values.

Sawyer and Li [116] proposed a versatile method that can be applied to any type of atmospheric profile data. Moreover, it takes advantage of the merits of the aforementioned techniques while overcoming their limitations. Figure 3 presents a comparison of the BLH detected by lidar, radiosonde and temperature profiles from a high-resolution infrared sounder. The BLH values derived from these different approaches agree generally well, although some consistent differences exist.

The mast or meteorological tower is an important observational platform used to continuously measure profiles of turbulent flux (latent and sensible heat), and profiles of the atmospheric mixing ratio within the lower part of the PBL at a reasonably high resolution [84,104,117,118]. The main shortcoming of this platform is its limited range, which is typically below 300 m. As a simple remote sensing instrument, the sodar is suitable for routine operations [104,119]. The sodar can capture typical PBL features by measuring structure parameters such as the acoustic refractive index, irrespective of stable or convective atmospheric conditions. With Doppler capability, it can determine vertical velocity variance profiles. For instance, Yang *et al.* [120] characterized the daytime evolution of the PBL based on observed vertical velocity variance profiles using one Doppler sodar on the Tibetan Plateau during the dry season. The sodar, however, is limited to an altitude range of 500–1000 m and is highly sensitive to environmental noise [104].

Boundary-layer wind profilers have been widely deployed in field campaigns to investigate the PBL structure [121–123] as well. Based on wind profiler measurements, the features of low-level jets in Shanghai and Tianjin have been elucidated by Du *et al.* [124] and Wei *et al.* [125], respectively. The wind profiler observed backscatter signals in clear air are proportional to the structure function parameter of the refractive index, which can be used to estimate the BLH under convective conditions [126,127].

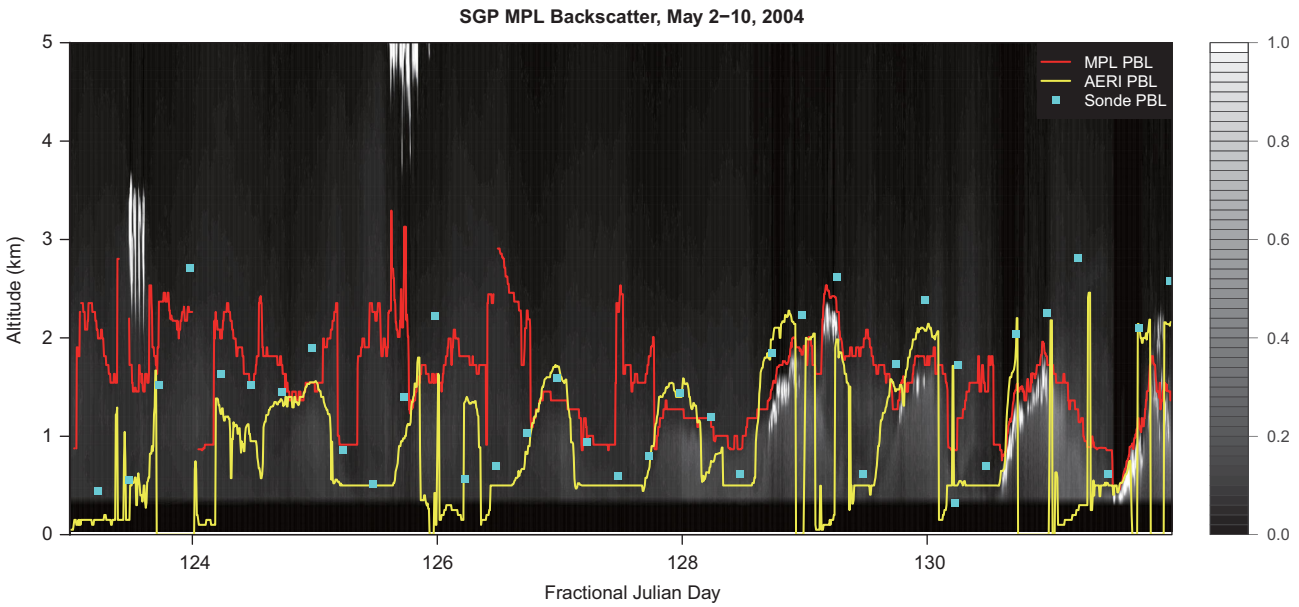


**Figure 3.** Evolution of BLHs calculated using micropulse lidar (MPL), atmospheric emitted radiance interferometer (AERI) and radiosonde data, overlaid on the MPL backscatter field during a nine-day period (2–10 May 2004) at the Southern Great Plains site in the US. (Adapted from [116].)

Orbiting around the Earth, the space-borne lidar has the unique merit of providing global BLHs. Using CALIOP-attenuated backscatter observations, the BLH was investigated over China by Liu *et al.* [128] and Zhang *et al.* [129], in the southeastern Pacific by Ho *et al.* [130], and over Europe by Leventidou *et al.* [131]. However, under stable PBL conditions, large uncertainties in estimating BLHs from space-borne lidar like CALIOP ensue due to the weak vertical gradients in the aerosol loading [104].

## PROCESSES GOVERNING AEROSOL AND PBL INTERACTIONS

### Aerosol-induced adiabatic heating in the PBL

To gain an insight into the radiative effect of aerosols on the PBL, it is essential to compute the radiative heating rate with known aerosol vertical extinction profiles and SSA profiles. The SSA profile is most difficult to get, although there are some aircraft *in situ* measurements of SSA. Several methods have been used to calculate the columnar SSA. One method is to use a combination of satellite-measured spectral reflectance and surface-measured transmittance, which can be collected over large regions such as across China [45]. Since the bulk of aerosols are well mixed in the PBL, one may assume to the first order of approximation that SSA derived for the entire atmospheric column is the same as that for the PBL. SSA values can then be used to compute the radiative heating rate by virtue of lidar-observed aerosol extinction or even backscattering profiles with certain assumptions regarding the backward scattering ratio [89]. Based on a single-channel elastic-scattering lidar, the backscattered radiation can be calculated according to the following equation [132,133]:

$$P(r) = O_c(r) C E \frac{\beta(r)}{r^2} \exp\left[-2\int_0^r \sigma(z)dz\right] + N_b + A(r), \quad (1)$$

where $r$ represents the range, and $\beta(r)$ and $\sigma(r)$ denote the backscattering and extinction coefficients caused by both aerosol and molecular factors, respectively. Other variables are detailed by Campbell *et al.* [132] and Welton *et al.* [71]. The normalized relative backscatter, $P_{\mathrm{NRB}}(r)$, or NRB, can be formulated as

$$P_{\mathrm{NRB}}(r) = C\beta(r) \exp\left[-2\int_0^r \sigma(z)dz\right], \quad (2)$$

where $C$ can be solved using a technique constrained by the co-located AOD at a range where molecular scattering is determined above the surface-detected aerosol layer under cloud-free conditions [71]. One can then solve for layer-averaged extinction–backscatter ratios and aerosol extinction coefficient profiles [71,134]. The radiative forcing of aerosols at the top, bottom, and within the atmosphere has been derived from this information [89]. The aerosol particles largely reside below 2 km AGL, most of which

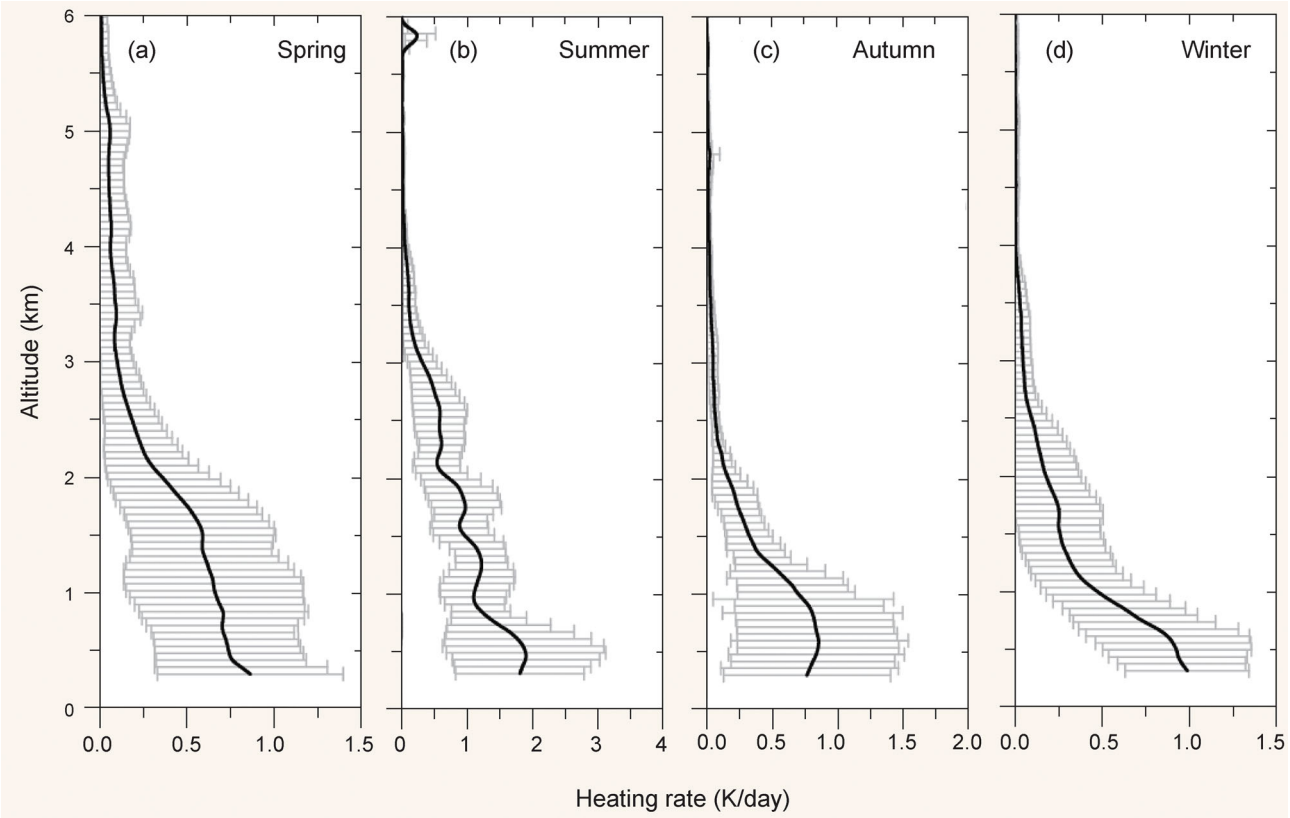


**Figure 4.** Seasonal daily averaged vertical profiles of aerosol particle heating rate (black solid lines), with their corresponding standard deviations (gray horizontal lines) at Taihu in the central Yangtze River Delta region of eastern China in (a) spring, (b) summer, (c) autumn and (d) winter during the period from June 2008 to May 2009. (Adapted from [89].)

(60%–80%) are within 1 km AGL. This results in large amounts of solar radiation trapped in the lowest part of the PBL, which in turn heats up the lower atmosphere (Fig 4).

## Aerosol–PBL interactions due to ARI

The strong contrast between warming and cooling in the atmosphere and the surface can drastically impact atmospheric stability and the PBL, which can affect weather and dynamics. By means of model (NCAR/CAM3) tests, it has been demonstrated that increases in aerosols of moderate absorption can reduce wind, weaken atmospheric circulation and even the monsoon system [7,135]. Accompanying the rapid degradation of air quality is the steady decrease in surface wind speed [136] that has been attributed at least partially to the effect of increasing aerosols, as shown in recent studies using long-term meteorological data [137,138].

Aerosols and the PBL interact inherently in a variety of ways [7,22,26,139]:

(1) Aerosols cool the surface and lower atmosphere by the reduction of shortwave, sensible heat, and latent heat fluxes.
(2) Absorbing aerosols above the PBL warm up the air of the free troposphere, and thus stabilize the boundary-layer inversion cap, inducing and prolonging the temperature inversion in the upper PBL, and suppressing diffusional dispersion of pollutants near the surface.
(3) Absorbing aerosols within the PBL may not strengthen the atmospheric stratification since there is strong vertical mixing in the PBL due to aerosol-induced atmospheric heating. Therefore, absorbing aerosol within the PBL does not naturally feed back to lower BLH. In this case, the lower BLH may be caused by the decrease of sensible heat at the surface.
(4) Aerosols weaken surface winds and atmospheric circulation within the PBL and increase atmospheric circulation above the PBL.

Long-term visibility data, a proxy for aerosol loading, have been used to infer the impact of aerosols on meteorological variables in the PBL [137,138,140]. Long-term (>50 years) trends in many meteorological variables were analyzed in central-western China, where aerosols are abundant and strongly absorbing [45]. By virtue of the special topography of the region (a large mountain range

and a broad plain), changes due to background dynamics (mountain stations), the aerosol or pollution effect (contrasting trends between mountain top and bottom), and urbanization (the big city of Xi'an and a rural station located on the plain) were successfully differentiated. Below are the major observational findings and conclusions that offer some clues about the potential influences of aerosols on the PBL and meteorological variables inside the PBL layer [137,138]:

(1) The difference in the daytime maximum temperature between plain stations (inside the PBL) and mountain-top stations (outside of the PBL) has decreased, implying cooling of the surface during the daytime, due presumably to aerosols.
(2) Wind speed has decreased over the plain stations, but increased at a neighboring mountain-top station, with the largest difference occurring around noon (most sensitive to aerosols), implying a trend of stabilization inside the PBL and destabilization outside the PBL. This has an important implication for the dispersion of pollutants from low lands, in particular, basins.
(3) The number of thunderstorms in the plains has decreased substantially, but little change is observed at the neighboring mountain-top station, implying weakening convection over the plains.
(4) The number of rainy days has decreased, implying the likely suppression of PBL clouds, which also has a bearing on the removal of pollutants by rain scavenging.

The finding of decreasing surface winds and increasing winds aloft is consistent with the hypothesis originally proposed by Jacobson and Kaufman [139] based on their model simulation with absorbing aerosols. The finding of decreasing thunderstorms is at odds with the aerosol invigoration effect, suggesting a dominant role of the aerosol thermodynamic effect due to strong aerosol absorption. The hypothesis was confirmed using Tropical Rainfall Measuring Mission (TRMM) thunder data in southeast China, where sulfate aerosols are more prevalent [140]. The trend is opposite to that found in central China, where aerosols are more strongly absorbing.

The effect of aerosols on atmospheric thermodynamics is more clearly revealed by the relationships between aerosol loadings and near-surface temperature inversions derived from continuous measurements from an atmospheric emitted radiance interferometer (AERI) deployed at the US Southern Great Plains site for over a decade. Atmospheric temperature profiles derived from the AERI have been used to study the climatology of temperature inversions [28]. It is expected that the thermal inversions in the lowest troposphere, especially near the ground, are substantially affected by aerosols, particularly absorbing ones. This was confirmed by the observed enhanced frequency of inversions with increasing aerosol loading but declining frequency of inversions with increasing aerosol SSA, as shown in Fig 5. This indicates that temperature inversions tend to occur at high and absorbing aerosol conditions. Among the absorbing aerosols, BC is one of the most important categories, accounting for ∼10%–50% of the total tropospheric aerosol particles. The atmospheric effects of BC largely refer to the interference with radiative transfer, visibility impairment, PBL stabilization, and alteration of cloud formation, which are strongly sensitive to the aging processes and mixing states with other aerosol constituents [141–143].

Comprehensive measurements of atmospheric chemical composition, the PBL, meteorological parameters and surface flux at ground-based stations provide opportunities to gain further insights into aerosol–PBL interactions [144]. Based on such measurements at the Station for Observing Regional Processes of the Earth System (SORPES), a 'golden' case that occurred on 10 June 2012 was studied by Ding *et al.* [15]. Compelling evidence of aerosol–PBL–weather interactions was revealed. A mixed layer of heavy biomass burning and urban pollution plumes substantially reduced the amounts of solar radiation, latent and sensible heat fluxes, and air temperature on the ground and in the lower PBL, which suppressed convection and the formation of a would-be major rain event in Nanjing. Increased hygroscopic effects related to increased RH associated with decreased air temperature [15] and a faster secondary aerosol formation [16] could enhance aerosol–meteorology interactions. By analyzing long-term continuous measurements of aerosols, radiation and fluxes at the SORPES station in Nanjing and guided by theory, quantitative relationships were established between PBL turbulence flux, aerosol concentration and RH [27]. Suppression of vertical turbulence mixing confined aerosols to a shallower PBL, causing a positive feedback loop between aerosols and the PBL that further lowers the BLH [145].

Intensive measurements made throughout the day help understand the aerosol–PBL relationship. For example, using vertical profiles of BC measured by a micro-aethalometer, Ran *et al.* [146] found weak turbulence and an inversion layer under high concentrations of aerosols in a shallow PBL. Aerosols were diluted by the fast development of the PBL and a uniform distribution of aerosols was typically observed during the daytime in an unstable PBL. In the evening, aerosols quickly build up near

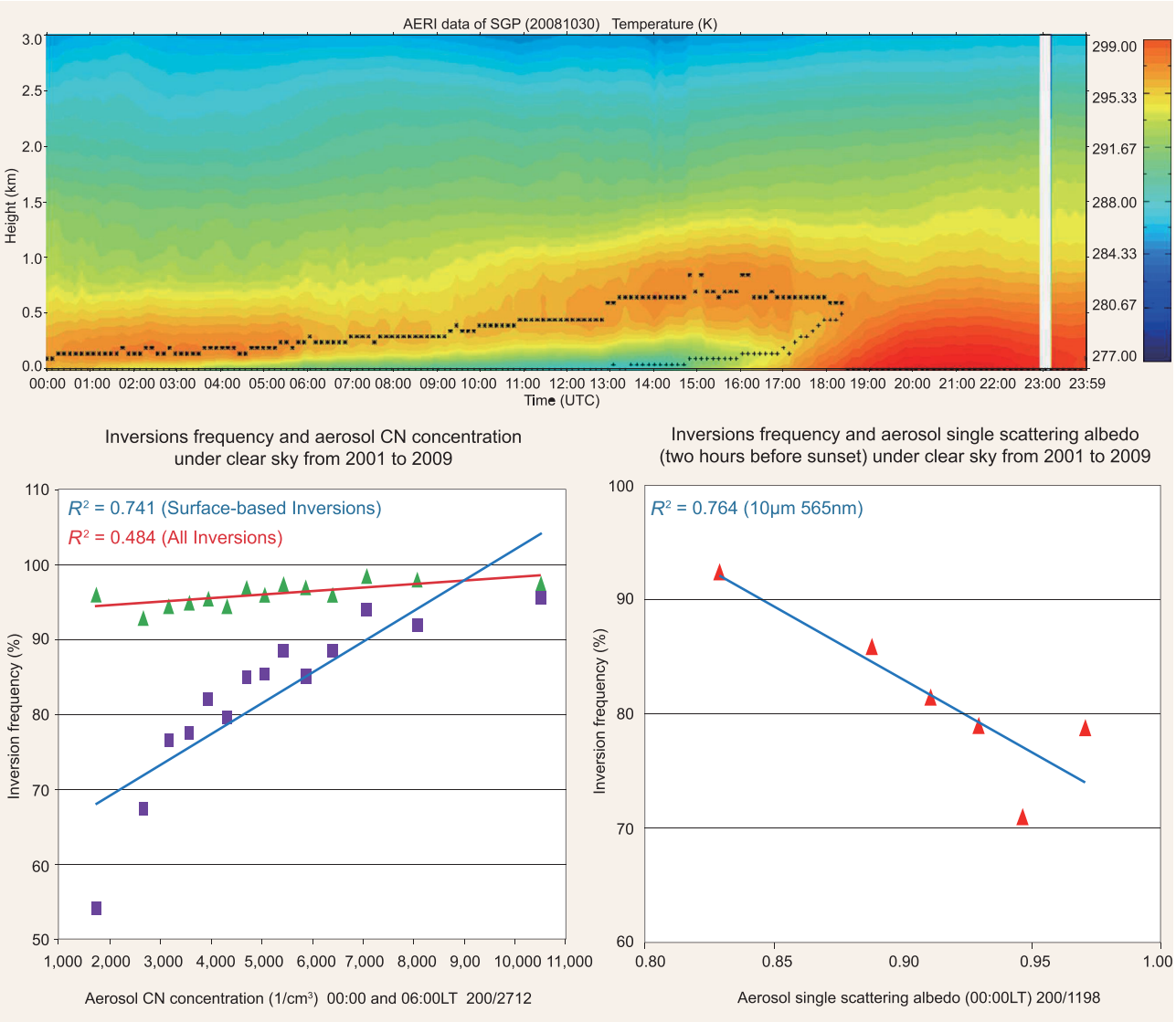


**Figure 5.** Impact of aerosol on temperature inversion in the lowest troposphere. Upper panel: A time series of temperature profiles retrieved from the atmospheric emitted radiance interferometer (AERI) measurements on 30 October 2008 over the US Southern Great Plains (SGP). Lower left: the frequency of occurrence of temperature inversion near the surface as a function of the number concentration of condensation nuclei (CN) derived from nine years of observations at the SGP site, which is part of the US Atmospheric Radiation Measurements (ARM). Lower right: same as the lower left panel but as a function of aerosol single scattering albedo. The method and dataset used are described in [28].

the surface and decline exponentially with height, followed by the collapse of the mixing layer and then the formation of a stable nocturnal boundary layer [146,147].

## Aerosol and convection interactions

PBL–aerosol interactions also affect convection, due to aerosol-induced changes in the atmospheric profile of heating, and surface latent and sensible heat fluxes that significantly affect the evolution of the boundary layer. Gu *et al.* [148] found that for East Asia, the modeled radiative impact of boundary-layer aerosols suppressed tropical convection. Convective potential available energy is controlled by boundary-layer temperature and humidity [149]. The source of energy for both the convective boundary layer and deep convective cells ultimately originates from surface heating and moisture [150,151]. The PBL also affects deep convection [3,152,153], especially if it hosts absorbing aerosols that can provide enhanced potential energy above the PBL [22].

Wang *et al.* [154] shows that absorbing aerosols residing in the PBL can destabilize the lower atmosphere at the periphery of tropical cyclones, enhance convection in the rainband region, but cut off the energy inflow to the eyewall. More recently, the conditional enhancement of instability by

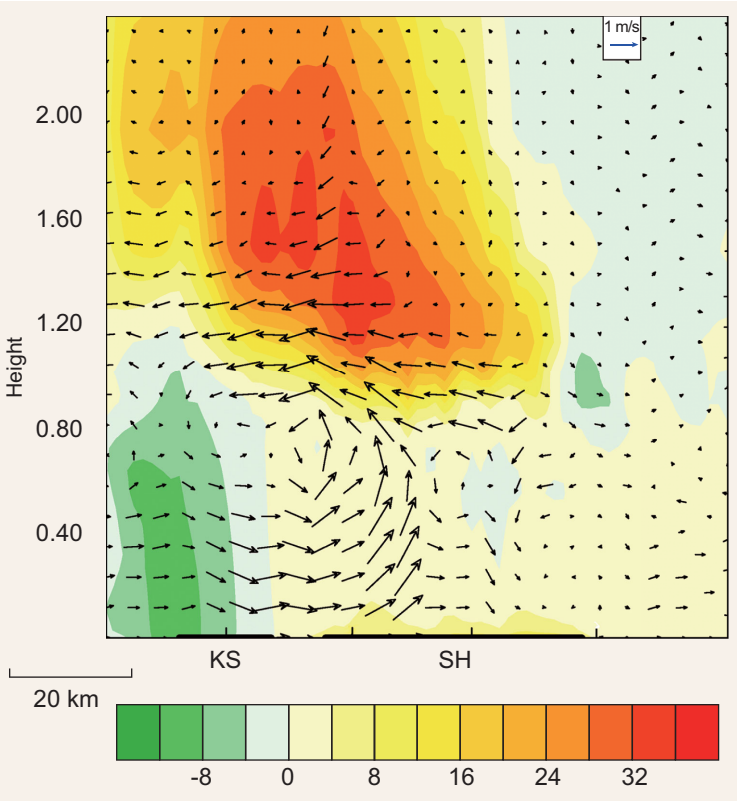


**Figure 6.** Vertical cross-section of the difference in simulated $O_3$ concentration (ppbv) and in-plane vectors, where the vertical speed is multiplied by a factor of 10, between urban land use and no urban land use in Shanghai simulations. (Adapted from [157].)

absorbing aerosols was simulated by Fan *et al.* [155] and Lin *et al.* [156]. In those simulations, due to the radiative heating caused by soot particles in the PBL, both relative humidity and convection strength associated with shallow cumuli are reduced during daytime. However, the altered daytime temperature and moisture conditions act to reserve the energy, thereby facilitating the development of nighttime deep convection.

## Aerosol–PBL–chemistry interactions

Variations in the macro- and micro-physics of the PBL may alter the photochemical and thermal chemical reaction conditions in the PBL and thus affect the near-surface air quality. Any variations in photolysis rate, temperature, humidity and concentration of species and structures of the PBL result in the adjustment of photochemical and thermal chemical reaction rates, the chemical equilibrium constant and even changes in chemical products. Moreover, small modifications of solar radiation, atmospheric stability and the structure of the PBL could induce significant changes in the chemical environment, for instance in the ozone photochemistry [157] or on new particle-formation processes [158,159]. Figure 6 shows that the circulations and boundary-layer structures over the downstream Kunshan are closely associated with the upstream urban surface (Shanghai), which further affects the $O_3$ concentration by redistributing $O_3$ and its precursors. To be specific, the horizontal transport of $O_3$ and its precursors, from upstream Shanghai to downstream Kunshan, are suppressed in the lower PBL but strengthened in the upper PBL due to the strong circulation caused by the urban heat island effect.

A significant attenuation (>50%) in ultraviolet (UV) radiation due to atmospheric aerosols in polluted and urban areas has been reported [160]. Such an attenuation of UV radiation by aerosols can exert a significant influence on photolysis and species chemical cycles, especially photochemical reaction processes. The brown carbon emitted from biomass burning diminishes UV-B radiation so strongly that it can reduce the net production rate of ozone by up to 18% and the mass concentrations of $HO_2$, radicals OH and $RO_2$ by up to 15%, 17% and 14%, respectively [161]. From observations and simulations using a radiative-transfer/air-quality model, UV-scattering particles in the PBL tend to accelerate photochemical reactions, as opposed to the inhibition effect caused by UV-absorbing aerosols [162]. The hygroscopic growth of aerosol particles normally occurs in polluted air with relatively high humidity, which can largely affect their SSA. In comparison with the dry state condition, the calculated $J_{NO2}$ at RH = 98% at 1 km AGL increased by 30.4% due to the UV radiation enhancement induced by the larger-sized humidified scattering aerosol particles [163]. The influence of aerosol hygroscopic growth on the $J_{NO2}$ profile inhibits photolysis at the surface and accelerates it in the upper PBL by a similar mechanism described by Dickerson *et al.* [162]. This amplification of $J_{NO2}$ in the upper PBL likely brings about high aerosol concentration and more ozone production in the polluted upper PBL and free troposphere [163].

The direct and indirect effect of aerosols can alter the photochemical reactions and ozone concentration [164–166]. For instance, absorbing aerosols were found to be able to reduce the photolysis rate and weaken ozone generation, while scattering aerosols showed opposite change [167,168]. Li *et al.* [169] found that PBL $O_3$ was reduced by 5% in highly polluted regions in summertime in Central Eastern China. Deng *et al.* [160] found that UV radiation/ozone is negatively correlated with $PM_{10}$, and at least half of the UV radiation was attenuated by the atmospheric aerosols. Li *et al.*, [170] found a reduction of about 2%–17% in surface ozone during the daytime in Mexico City due to the changes in

photolysis rates caused by aerosols. The simulation by Cai *et al.* [171] shows that an elevated concentration of particulate matter can increase the AOD by 20%–40% and reduce photolysis rates of $NO_2$ and $O_3$ by 20%–30%, resulting in a reduction of 30%–40% in the net photochemical production rate of $O_3$.

Aerosols also exert an important influence on ozone concentrations by heterogeneous reactions. Ravishankara [172] determined the role, rates and media of heterogeneous reactions in the troposphere. Jacob [173] proposed that heterogeneous reactions have an impact on $O_3$ concentrations by affecting generation and consumption of $NO_x$, $HO_x$, $O_3$ and halogen radicals. Heterogeneous reactions on sea salt and soot surfaces have significant effects on the trace gas [174–177]. Kleffmann *et al.* [178] and Kaiser *et al.* [179] noted that BC has relatively larger surface area, favoring heterogeneous chemistry.

Liao and Seinfeld [180] found that the surface $O_3$ concentrations in eastern China can be reduced by 25%–30% because of the heterogeneous reactions on wet surfaces of sea salt, nitrate, sulfate, ammonium, mineral dust and organic carbon aerosols. Overall, the heterogeneous reactions reduce annual mean $O_3$ in eastern China by 10%–18% [182]. These reactions take up ozone precursors such as $NO_x$ and $N_2O_5$, leading to reduced $O_3$ concentrations, which explains in part why $O_3$ concentrations have kept increasing while $PM_{2.5}$ concentrations have decreased, which has been happening in China in recent years as a direct result of emission control measures for aerosols. Note that the impact of heterogeneous processes is strongly dependent on aerosol concentrations and the surface uptake coefficients [181]. Heterogeneous reactions also likely play a central role in the formation of major aerosol ingredients, including sulfate, nitrate and organics [183–185].

Urbanization also affects local and downstream air quality in two major ways. First of all, land surface properties and meteorological fields modified by urban canopies alter the chemical reaction, dry and wet depositions, and the spatial distribution of primary and secondary atmospheric pollutants. Second, urbanization processes tend to enhance local human activities, thereby scaling up anthropogenic emissions. Both pathways will exert non-negligible influences on air quality on local and regional scales. Zhang *et al.* [186] showed that without an upstream city, the urban heat island (UHI) effect over Baltimore would be 1.25°C weaker and the PBL would be 200 m shallower, which could redistribute the air pollutants throughout Baltimore. Anthropogenic heat emissions can significantly change the UHI and urban-breeze circulations in cities in the Yangtze River Delta region, which in turn changes the spatial and vertical distributions of the simulated air pollutants [187]. Urban aerosols may also contribute to the UHI based on satellite observations and urban climate simulations [188]. The urban–rural difference in haze pollution levels is one of the key factors determining nighttime UHI across China.

Rapid vertical mixtures in the convective boundary layer (CBL), along with a temperature-dependent partitioning of atmospheric nitrate between the gas and aerosol phases, results in complex interactions between dynamics and aerosol formation [189]. Near the top of the CBL (cooler), gaseous nitric acid and ammonia condense on ammonium nitrate and the gas–aerosol equilibrium shifts towards the aerosol phase. Close to the surface (warmer), ammonium nitrate evaporates into gaseous nitric acid and ammonia, shifting the equilibrium towards the gas phase. Using a large-eddy simulation (LES) model coupled with radiation, chemistry and the surface exchange of aerosols, Barbaro *et al.* [190] highlighted that the close connection of the gas–aerosol conversion of nitrate to CBL (thermo-)dynamics produces highly nonlinear concentration and vertical profiles of turbulent flux.

Although a great deal of phenomena related to aerosol–PBL–chemistry interactions have been reported, most of the explanations for the underlying mechanisms are qualitative and a deeper insight is still warranted.

## Aerosol, PBL and cloud interactions

The interactions between cloud-nucleating aerosols and the PBL involve complex feedbacks between cloud microphysics, precipitation and PBL turbulence. Precipitation is a key component regulating the PBL evolution. When the aerosol concentration increases, more but smaller cloud droplets are formed and precipitation is suppressed [2], leading to significant changes in PBL evolution [191–193].

In a stratocumulus-topped PBL, the effects of heavy drizzle on PBL turbulence and structure were simulated with a LES model developed by Stevens *et al.* [191]. Significant evaporative cooling in the sub-cloud layer ensued and weakened mixing from the cloud layer to the sub-cloud layer. Less turbulent kinetic energy (TKE) was generated in the PBL, leading to a weaker cloud-top entrainment. As a result, the growth rate of the PBL was slowed down and the PBL became thinner. PBL turbulence and cloud-top entrainment can become significantly stronger with increasing aerosols [193]. The growth rate of a stratocumulus-topped PBL increases with aerosol loading. Because the air in the inversion layer

above the PBL is normally warm and dry, the enhanced cloud-top entrainment can cause warming and drying of the PBL and reduce the cloud liquid water path (LWP) [194].

However, in a stratocumulus case with very weak drizzle, the evaporative cooling and moistening right below the clouds can create instability for the sub-cloud layer. The weak drizzle then helps to produce TKE in the PBL. When aerosols are increased, the reduced drizzle results in weaker PBL turbulence [192]. This is because there is less evaporative cooling and less moistening below clouds, and therefore weaker instability in the sub-cloud layer. The PBL then has a less effective supply of surface water vapor to clouds and therefore a much lower LWP. The reduced drizzle in the high cloud condensation nuclei case is believed to weaken the coupling between the surface and air in the PBL, and to reduce the vertical fluxes of heat and the transport of water vapor. This weakens any cloud development that may ensue.

In a cumulus-topped PBL, the aspect ratio, the turbulent mixing process, cloud organization and formation mechanisms of shallow cumulus clouds all differ from the stratocumulus cloud case. As cumulus clouds introduce liquid water into the inversion layer, the subsequent evaporation provides moisture and the dry inversion-layer air gradually becomes moist and takes on the characteristics of the cloud layer, therefore deepening the PBL [195]. Also, the non-precipitating cumulus-topped PBL grows proportionally with time. It was hypothesized that the precipitation from shallow cumulus can arrest the growth of the PBL by the removal of liquid water from the cloud top. However, to what extent the aerosol-induced changes in precipitation can affect the PBL growth rate has not been well studied.

As aerosols increase in the cumulus-topped PBL, PBL turbulence is affected by two processes. Xue and Feingold [196] described one process in which increasing aerosols results in smaller cloud droplets, and therefore faster evaporation at the cloud top and edges. The faster evaporation tends to generate stronger evaporative cooling and stronger downdrafts at cloud edges, which produces more TKE and enhances the evaporation of the clouds. This results in a smaller cloud fraction and thinner clouds. In another process described by Grabowski *et al.* [197], increasing aerosols leads to precipitation suppression, less efficient condensate removal, and therefore weaker buoyancy due to the water loading, resulting in shallower clouds. Although both of the mechanisms suggest shallower clouds under higher aerosol-loading conditions, their underlying reasons are completely different.

The patchy precipitation in cumulus clouds can cause a temperature anomaly (cold pool) and a moisture anomaly (more moisture) in the sub-cloud layer [198]. The evaporative cooling and associated downdrafts lead to divergence at the center of the precipitating cells at the surface and convergence at the edges of the precipitating cells. This facilitates the formation and development of new clouds, resulting in a mesoscale open cellular structure [199,200]. In the polluted case, increased aerosols can suppress precipitation and the formation of open cellular structures.

In a cumulus-topped PBL, cumulus clouds are also very efficient at vertically transporting aerosols [201]. When the source is at the surface, aerosols are transported upwards mainly through the updraft regions of cumulus clouds. When the source is in the inversion layer, which means that aerosols are transported to the studied region by the free atmosphere, aerosols can be transported downward mainly in the downdrafts of the shell regions of cumulus clouds.

In summary, most studies have shown that increasing aerosols can suppress precipitation, as expected from the traditional theory of cloud microphysics. However, it has feedbacks to PBL turbulence, surface processes and radiation through several pathways. Further studies are needed to reveal the mechanisms underlying these interactions in the PBL.

## THE TREND AND FLUCTUATION OF AIR POLLUTION: THE ROLES OF CIRCULATION, PBL, CLIMATE CHANGE AND WEATHER

Concentrations of pollutants (aerosols and precursor gases) are driven by emission, transformation (e.g. gas to particle conversion), transport and deposition. These drivers may be classified as being chemical (e.g. the availability of oxidants), meteorological (e.g. wind speed, temperature, humidity, precipitation, soil moisture, solar radiation) and biological (e.g. vegetation cover and properties), etc. While all these factors are at work in dictating air pollution at any time and location, we argue that the following factors are most essential:

(1) Emissions of precursor gases, primary and secondary aerosol particles;
(2) Gas-to-particle, or new particle formation and growth;
(3) Large-scale circulation and local-scale aerosol–PBL interactions;
(4) Long-term climate change;
(5) Weather regimes.

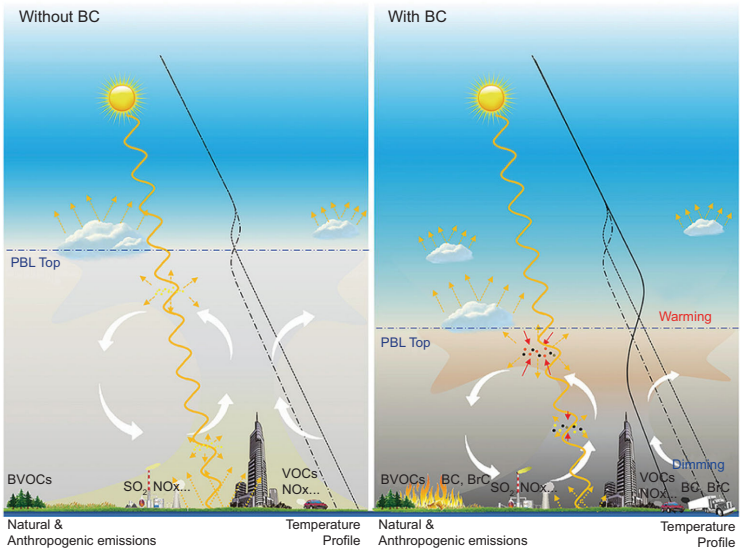


**Figure 7.** A schematic figure showing the aerosol–boundary-layer feedback loop for scenarios without (left) and with (right) black carbon (BC) emissions in a megacity. The black lines give air temperature profiles (solid, dotted and dash-dotted lines for the scenarios with BC, without aerosols, and with aerosols except for BC, respectively). The yellow dashed lines with arrows denote the reflection of solar radiation by the ground surface, clouds and aerosols. The red arrows show absorption of solar radiation by absorbing aerosols. The blue dash-dotted line indicates the top of the PBL. White arrows show the vertical ventilation of urban plumes induced by circulations or large eddies induced by the urban heat island effect. (Adapted from [24].)

Since the first two topics will be addressed in separate review articles of the same special issue, we will just elaborate more on (3) to (5).

## Large-scale circulation and local-scale aerosol–PBL interactions

Air pollution is intimately related with large-scale circulation and local-scale aerosol–PBL interactions [66,202–207]. High-resolution mesoscale meteorological models, e.g. the MM5 and the WRF, have been widely used to study their joint roles. For example, MM5 simulations suggested that the evolution of sea–land breezes and PBL dynamics were influenced by an approaching northwest Pacific typhoon [205]. Based on WRF-FLEXPART simulations, it was found that the PBL air pollutants from the North China Plain can be transported by cyclones and its associated warm conveyor belts to the free troposphere over Northeast China [206]. This study showed that Lagrangian modeling connected to high-resolution meteorological output from mesoscale models could well demonstrate detailed air pollution transport and dispersion mechanisms under specific synoptic weather conditions. Also, based on offline air-quality models [208,209], many previous studies have been conducted to understand PBL aerosols and their impacts in typical regions of China under different synoptic conditions [210–215].

In comparison with 'offline' air-quality models that often underestimate extreme aerosol peaks during severe haze episodes [215], 'online' coupled models considering the aerosol–radiation–PBL–weather feedback can improve the forecast capabilities of severe pollution events taking place in Beijing during wintertime [216,217]. For the WRF-Chem simulation with mixed biomass burning with urban plumes [15], it showed that daytime mixed biomass burning plumes not only 'burn off' daytime precipitation but also enhance nighttime precipitation in downwind regions [218]. It was also found that dust aerosols from Northwest China could have a strong aerosol–PBL feedback and influence the PBL structure along transport pathways, which could even influence the emission and deposition of dust in the source and downwind regions [219].

Using the online-coupled WRF-Chem numerical model, Ding *et al.* [24] first singled out the role of BC aerosol and PBL interactions in polluted events and attributed an extreme haze episode in East China to the positive feedback between absorbing aerosol and PBL. The feedback tends to lower the BLH, which was thus referred to as the 'dome effect', as illustrated in a simplified conceptual scheme (Fig 7) that is valid under the static state of the PBL. Under general conditions, mixing takes place due to any inhomogeneous heating of the atmosphere. The extra heating by aerosol absorption in the upper PBL may be mixed down into the interior of the PBL to lower the PBL.

The hypothesized 'dome effect' seems to prevail even on the decadal trend of AOD retrieved from satellites (MODIS and MISR) at different altitudes. As shown in Fig 8a, Dong *et al.* [145] found opposite trends for AOD: decreasing and increasing below and above ∼0.5 km in northern China, which is dominated by strong absorbing aerosols with low SSA (45). The increase in the lower PBL is a testimony to the positive feedback caused by a reduced temperature lapse rate or even inversion that keeps pollutants accumulating, whereas above the layer of maximum absorption conditions the PBL becomes more unstabilized and more favorable for diffusional transport of pollutants. As such, even though the overall basin-wide column total AOD may not have changed much, the aerosol loading near the surface in the center of the basin has increased drastically. To reinforce the argument, they also analyzed similar trends in southern China (cf. Fig 8), where aerosols are generally less absorbing and thus weaker feedback takes place. The trends of AOD at different altitudes are much more consistent with little

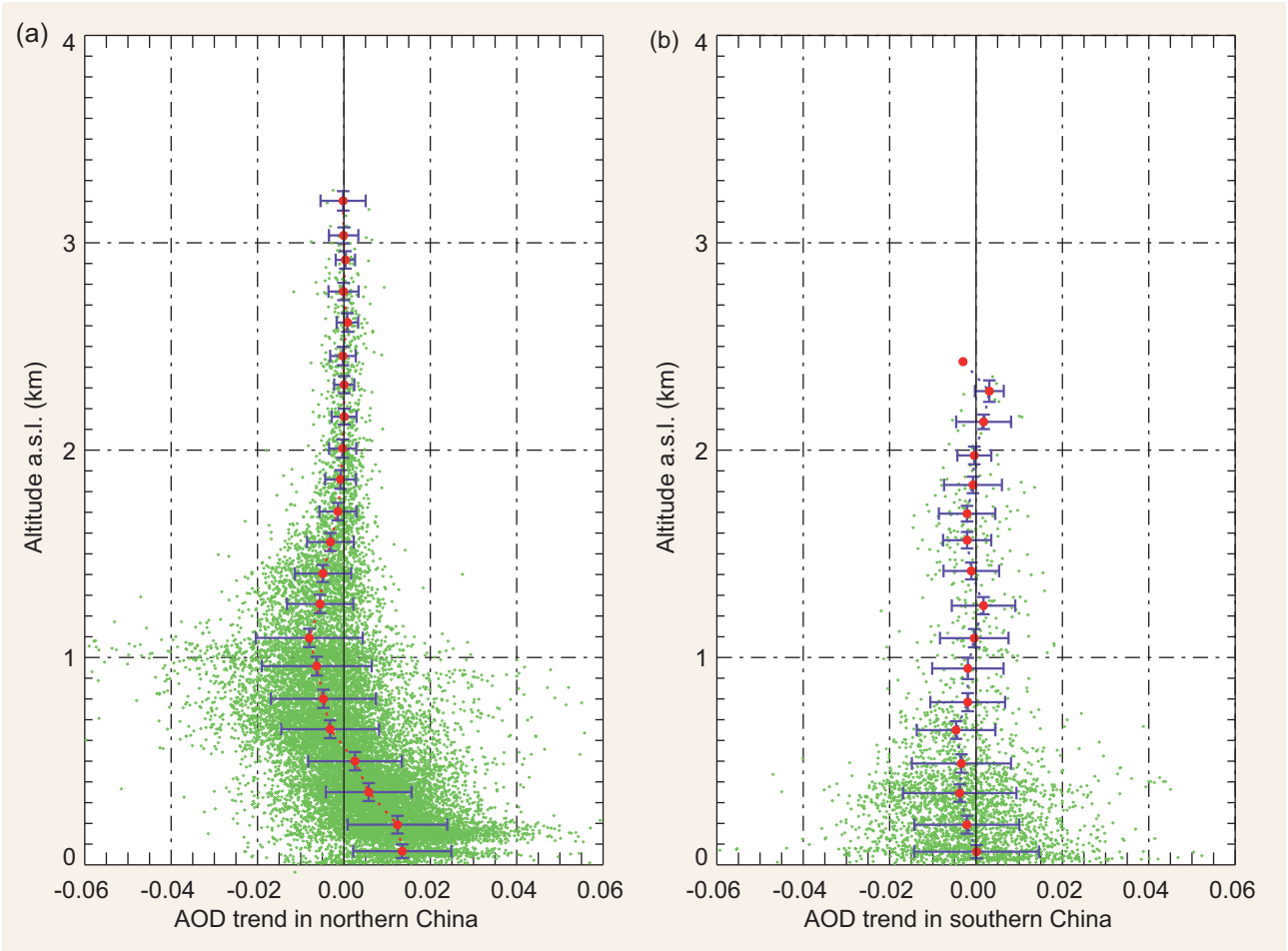


**Figure 8.** The vertical profiles of AOD trends over the period of 2002–2014 as a function of altitude above sea level in northern (low SSA) and southern (high SSA) China derived from MODIS AQUA. (Adapted from [145].)

change, due presumably to the lack of the positive feedback process.

These findings suggest that absorbing aerosols not only alter atmospheric thermodynamics and stability, but can also effectively push down the BLH to severely exacerbate air pollution near the surface. Apparently, such a deterioration of air quality has little to do with the emission of pollutants, but more to do with their accumulation in a thinning PBL. This could be an important mechanism that ought to be accounted for in understanding and forecasting air pollution.

The mechanism may also help explain the systematic difference in the PBL height between the US South Great Plains and Hefei, Anhui, China, as shown in Fig. 9. The two sites have somewhat similar meteorology, but aerosol concentrations and types are distinctly different. AOD is much larger at Hefei than at the SGP, and the opposite is true for the PBL height. Besides, aerosols in China are generally more absorbing than the rural area of US due to much less consumption of coal.

The mechanism governing aerosol and PBL interactions for absorbing aerosols is illustrated in Fig. 10. As a result of reduction in surface fluxes and atmospheric heating, the lapse rate decreases and probability of inversion increases. These are unfavorable for the dispersion of pollutants that would further enhance atmospheric stability, etc.

## Aerosols and climate change

Increased temperature can enhance the chemical production of sulfate [220] but reduce nitrate formation through shifting gas–particle equilibrium [221,222]. All aerosol species are found to be very sensitive to changes in precipitation scavenging [223–225]. As such, understanding of any long-term changes in air pollution must take into account the changes in climate [6,7], as well as the day-to-day change in air quality [103]. In Asia, the monsoon is the most important dynamic regime dictating the Asian atmospheric environment whose changes are key to understanding any long-term trend of air

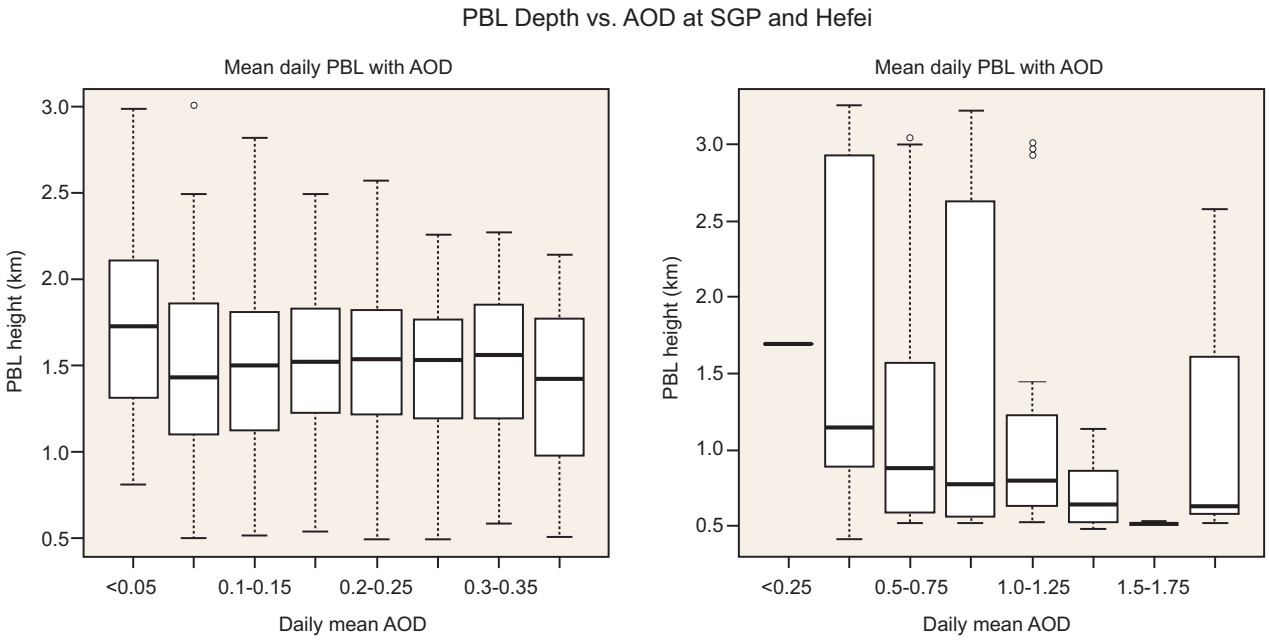


**Figure 9.** Boxplots showing the distribution of PBL depths with increasing AOD, at SGP (left) and Hefei (right). Adapted from the Ph.D dissertation of V. Sawyer (2015).

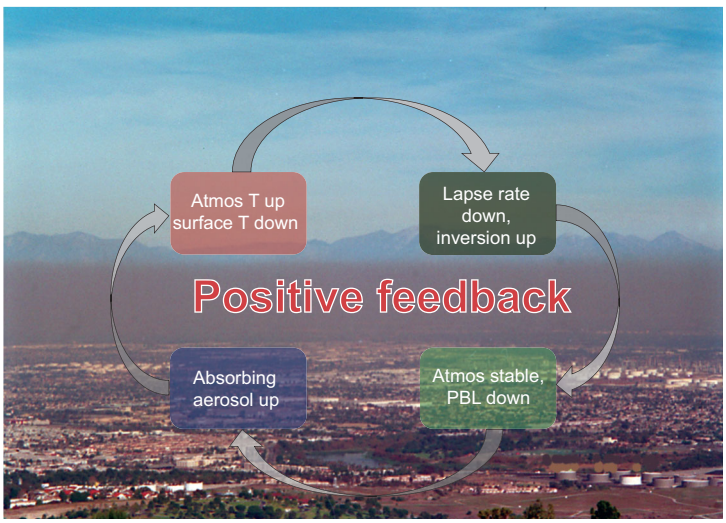


**Figure 10.** The mechanism of a positive feedback between absorbing aerosol and PBL interactions. T: temperature; Atmos: Atmospheric.

pollution [7]. On the other hand, climate changes in Asia, especially in China, are also strongly affected by anthropogenic activities.

Climate change influences aerosol concentrations in China on different timescales, including seasonal [226], interannual [135,227–230] and decadal variations [135,227,231,232]. Summer monsoon rainfall, cross-equatorial flows that carry clean air from the oceans and the relatively higher BLH lead to generally lower aerosol concentrations in summer than in winter [226]. In North China (32–42°N, 110–120°E), interannual variations of 11%−17% relative to the mean pollution concentrations were simulated over 2004−2012 [228], indicating that the aerosol effect on the PBL could vary greatly year by year. As special cases of aerosol interannual variations, seasonal mean aerosol concentrations in eastern China have been reported to correlate negatively with East Asian monsoon strength for both summer and winter [7,135,227]. For decadal variations of aerosols, Yang *et al.* [231] reported that, although changes in anthropogenic emissions dominated the increasing trend in wintertime $PM_{2.5}$ concentrations over eastern China, variations in meteorological parameters contributed 17(±14)% to the overall increasing trend in $PM_{2.5}$ concentrations in this region from 1985 to 2005.

Climate change also influences severe fog and haze events, especially in northern China in winter. Niu *et al.* [135] found that decadal and persistent decreases in visibility were associated with a long-term reduction in cold-air outbreaks from Siberia, and an increase in calm or low-wind days, which were further attributed to global warming by means of global climate model (GCM) simulations [135]. Cai *et al.* [59] developed an effective haze weather index to represent such favorable weather conditions by using observed long-term $PM_{2.5}$ daily concentrations at Beijing and daily reanalysis of meteorological fields, and showed that favorable weather conditions for severe haze increased by 10% over 1982–2015 relative to 1948–1981, owing to global warming by greenhouse gases. Other studies also showed consistent conclusions. As a result of global

warming, reductions in Arctic sea-ice cover correlated with the increases in wintertime haze days in northern China [60,233], and reduced mineral dust aerosol emissions led to more stagnant conditions favorable for haze days over eastern China [234]. In addition to climate change by anthropogenic forcing, natural climate variability was found to influence haze days. Decadal variability in the occurrence frequency of wintertime haze in central eastern China was reported to be closely associated with the Pacific Decadal Oscillation [235].

## Aerosols and weather regimes

The vertical distribution of aerosol particles is significantly affected by meteorological conditions [66,236] such as convective transport and removal processes [237], and the PBL structure and processes [238–242]. Aerosol concentrations and effective radii typically differ within and above the PBL since the BLH and the intensity of the turbulence affect to some degree the 3D distribution of air pollutants [243,244]. It has been observed that fine particles ($< 2.5\ \mu$m in aerodynamic diameter) tend to be well mixed vertically during the daytime while coarse particles tend to reside close to the ground and surface due to gradation settling [245].

Modeling studies have suggested that the vertical distribution of aerosols tends to be modulated by local atmospheric circulations [241,246,247] such as mountain-valley breeze circulation and sea-breeze circulation. In mountain-valley/plain regions, the presence of a mountain-valley breeze circulation can modify the PBL structure over valleys/plains through dynamic advection and the accompanying thermal alteration [241,248,249]. Meanwhile, the upslope wind of a valley breeze circulation may bring aerosols to the top of the PBL and form an elevated pollution level there [246,250,251]. In coastal regions, the updraft induced by the frontal movement of a sea breeze may also bring near-surface aerosols to the top of the PBL [241,252,253].

## CONCLUDING REMARKS

The PBL involves a number of chemical, physical and dynamic processes that are closely related to the accumulation of aerosol pollution, dispersion and transport. There are complex interactions between aerosol and PBL that jointly dictate air pollution. PBL–aerosol interactions and their feedbacks on meteorology thus complicate the forecasting of air quality.

This paper presents a comprehensive review of aerosols, the PBL, their interactions and impact on air quality. While we have learned a great deal on all pertinent fronts, there is still a wide range of fundamental PBL characteristics or key boundary-layer processes that are poorly understood or overlooked. Most work related to PBL processes is based primarily on time series of measurements made at fixed sites chiefly through field experiments that have a poor spatial coverage. A dense network of both aerosol and meteorological measurements is urgently needed to gain an explicit insight into the evolution of the PBL and the roles of aerosols played in combination with atmospheric processes driven by both large-scale and local-scale processes. This would improve PBL parameterizations and turbulence closures used in the models. A major challenge lies in the observation of the vertical profiles of atmospheric variables and aerosol properties, none being trivial at present but essential to improve our understanding of aerosol–PBL interactions. This requires more state-of-the-art ground-based and airborne measurements in different regions. For example, the BLH is a key variable whose observation is still far from being adequate. Sounding balloons are generally launched twice per day, making it impossible to study the diurnal variation of the PBL during a day, whereas space-borne lidar has a low signal–noise ratio, and thus very large uncertainty, due to strong attenuation, besides being available at nadir view only. Likewise, there is a severe dearth of vertical profile measurements of aerosol absorption that is the key for aerosol–PBL interactions.

In addition to boundary-layer measurements, PBL modeling efforts such as explicit PBL schemes have to be improved in operational weather or climate models. Current aerosol–climate models are able to simulate aerosol–climate interactions on seasonal, interannual and decadal timescales, but few studies have examined the changes in PBL from climate simulations. Attention has mostly been paid to atmospheric temperature, circulation and precipitation in a changing climate. PBL schemes are generally included as sub-models in atmospheric chemistry models, and numerical weather or climate prediction models, and are typically limited to a certain scenario. The coarse horizontal and vertical resolutions of climate models prohibit the accurate representation of boundary-layer processes. Many PBL schemes were developed mainly for applications in low-resolution models. These schemes would be difficult to apply to increasingly high-resolution models that require more detailed and explicit representations of physical processes and physiographical features. Considering that climate models are moving forward to higher resolutions, accurate representations of land use, sub-grid thermal and dynamical structures, as well as the radiative effects of aerosols on the boundary layer, are the keys to

improving simulations of boundary layer, air quality and climate. Continual development of PBL models and parameterization schemes is thus highly recommended. Forecasting of air quality may be improved significantly by accounting for the aerosol–PBL interactions, which further require both aerosol loading and aerosol-absorption property, including its vertical distribution.

While the aerosol–PBL interaction plays a key role in air pollution, it is by no means the sole mechanism dictating air pollution, which is affected by a lot of different mechanisms and processes, but they are not the foci of this review. Other pertinent factors and their associations with aerosol pollution are pursued in other review papers, such as the effects of new particle formation [25], and large-scale circulation associated with monsoon systems [7].

## ACKNOWLEDGEMENTS

We thank Prof. Tong Zhu for his invitation to write this review article. We also appreciate the efforts made by J. Li, who helped generate Fig. 5.

## FUNDING

The majority of the authors are supported by the National Haze Research Program of the Natural Science Foundation of China (91544217, 91544229, 91544230, 91544231 and 91744207), the National Basic Research Program on Global Change (2013CB955804), the National Natural Science Foundation of China (41471301 and 41771399), National Science Foundation of US (5245880), and Chinese Academy of Meteorological Sciences (2017Z005).

## REFERENCES

1. Twomey S. The influence of pollution on the shortwave albedo of clouds. *J Atmos Sci* 1977; **34**: 1149–52.
2. Albrecht BA. Aerosols, cloud microphysics, and fractional cloudiness. *Science* 1989; **245**: 1227–30.
3. Rosenfeld D, Lohmann U and Raga GB *et al.* Flood or drought: how do aerosols affect precipitation? *Science* 2008; **321**: 1309–13.
4. Ramanathan N, Lukac M and Ahmed T *et al.* A cellphone based system for large-scale monitoring of black carbon. *Atmos Environ* 2011; **45:** 4481–7.
5. Boucher O, Randall D and Artaxo P *et al.* Clouds and aerosols. In Stocker T, Qin D and Plattner G-K *et al.* (eds). *Climate Change 2013: The Physical Science Basis. Contribution of Working Group I to the Fifth Assessment Report of the Intergovernmental Panel on Climate Change*. Cambridge:Cambridge University Press, 2013, 571–658
6. Liao H, Chang W and Yang Y. Climatic effects of air pollutants over China: a review. *Adv Atmos Sci* 2015; **32**: 115–39.
7. Li Z, Lau WKM and Ramanathan V *et al.* Aerosol and monsoon climate interactions over Asia. *Rev Geophys* 2016; **54**: 866–929.
8. Guo J, Deng M and Lee SS *et al.* Delaying precipitation and lightning by air pollution over the Pearl River Delta. Part I: Observational analyses. *J Geophys Res Atmos* 2016; **121**: 6472–88.
9. Wang Y, Wan Q and Meng W *et al.* Long-term impacts of aerosols on precipitation and lightning over the Pearl River Delta megacity area in China. *Atmos Chem Phys* 2011; **11**: 12421–36.

**Appendix 1:** List of acronyms and abbreviations used in this paper.

| Acronyms | Full name |
|---|---|
| ACI | Aerosol–cloud interaction |
| AERI | Atmospheric emitted radiance interferometer |
| AOD | Aerosol optical depth |
| ARI | Aerosol–radiation interaction |
| BC | Black carbon |
| CALIOP | Cloud–aerosol lidar with orthogonal polarization |
| CBL | Convective boundary layer |
| EAST-AIRE | East Asian Study of Tropospheric Aerosols: an International Regional Experiment |
| HOPE $J^3A$ | Haze Observation Project Especially for Jing-Jin-Ji Area |
| LES | Large-eddy simulation |
| MODIS | Moderate resolution imaging spectroradiometer |
| MPH | Maximum probability height |
| $N_a$ | Aerosol Number Concentration |
| PBL | Planetary Boundary Layer |
| PRIDE-PRD | Program of Regional Integrated Experiments of Air Quality over Pearl River Delta |
| RH | Relative humidity |
| SORPES | Station for Observing Regional Processes of the Earth System |
| SSA | Single scattering albedo |
| TI | Temperature inversion |
| TKE | Turbulent kinetic energy |
| UHI | Urban heat island |

10. Dockery DW and Pope CA. Acute respiratory effects of particulate air pollution. *Annu Rev Publ Health* 1994; **15**:107–32.
11. Anenberg SC, Horowitz LW and Tong DQ *et al.* An estimate of the global burden of anthropogenic ozone and fine particulate matter on premature human mortality using atmospheric modeling. *Environ Health Perspect* 2010; **118**:1189–95.
12. Holloway AM and Wayne RP. *Atmospheric Chemistry*. Cambridge: *Royal Society of Chemistry*, 2010.
13. Li Z, Xia X and Cribb M *et al.* Aerosol optical properties and their radiative effects in northern China. *J Geophys Res* 2007; **112**: D22S01.
14. Ramanathan V, Crutzen PJ and Mitra AP *et al.* The Indian Ocean Experiment and the Asian Brown Cloud. *Curr Sci* 2002; **83**: 947–55.
15. Ding AJ, Fu CB and Yang XQ *et al.* Intense atmospheric pollution modifies weather: a case of mixed biomass burning with fossil fuel combustion pollution in eastern China. *Atmos Chem Phys* 2013; **13**:10545–54.
16. Xie Y, Ding A and Nie W *et al.* Enhanced sulfate formation by nitrogen dioxide: implications from in situ observations at the SORPES station. *J Geophys Res Atmos* 2015; **120**: 12679–94.
17. Wang G, Zhang R and Gomez M *et al.* Persistent sulfate formation from London Fog to Chinese haze. *Proc Natl Acad Sci USA* 2016; **113**: 13630–5.
18. Cheng Y, Zheng G and Wei C *et al.* Reactive nitrogen chemistry in aerosol water as a source of sulfate during haze events in China. *Sci Adv* 2016; **2**: e1601530.
19. Jacobson MZ. Strong radiative heating due to the mixing state of black carbon in atmospheric aerosols. *Nature* 2001; **409**: 695–7.
20. Li Z, Lee KH and Xin J *et al.* First observation-based estimates of cloud-free aerosol radiative forcing across China. *J Geophys Res* 2010; **115**: D00K18.
21. Bond TC, Doherty SJ and Fahey DW *et al.* Bounding the role of black carbon in the climate system: a scientific assessment. *J Geophys Res Atmos* 2013; **118**: 5380–552.
22. Wang Y, Khalizov A and Zhang R. New directions: light absorbing aerosols and their atmospheric impacts. *Atmos Environ* 2013; **81**: 713–5.
23. Peng J, Hu M and Guo S *et al.* Markedly enhanced absorption and direct radiative forcing of black carbon under polluted urban environments. *Proc Natl Acad Sci USA* 2016; **113**: 4266–71.
24. Ding AJ, Huang X and Nie W *et al.* Enhanced haze pollution by black carbon in megacities in China. *Geophys Res Lett* 2016; **43**: 2873–9.
25. Zhang R, Khalizov AF and Wang L *et al.* Nucleation and growth of nanoparticles in the atmosphere. *Chem Rev* 2012; **112**: 1957–2011.
26. Yu H, Liu SC and Dickinson RE. Radiative effects of aerosols on the evolution of the atmospheric boundary layer. *J Geophys Res* 2002; **107**: 4142.
27. Petäjä T, Jarvi L and Kerminen VM *et al.* Enhanced air pollution via aerosol-boundary layer feedback in China. *Sci Rep* 2016; **6**: 18998.
28. Li J, Chen H and Li Z *et al.* Low-level temperature inversions and their effect on aerosol condensation nuclei concentrations under different large-scale synoptic circulations. *Adv Atmos Sci* 2015; **32**: 898–908.
29. Daugherty RL. The control of air pollution, a progress report on smog control in Los Angeles county. *Eng Sci* 1960; **4**: 898–908.
30. Malek E, Davis T and Martin RS *et al.* Meteorological and environmental aspects of one of the worst national air pollution episodes (January, 2004) in Logan, Cache Valley, Utah, USA. *Atmos Res* 2006; **79**: 108–22.
31. Silva P, Eric J and Vawdrey L *et al.* Fine particle concentrations and composition during wintertime inversions in Logan, Utah, USA. *Atmos Environ* 2007; **41**: 5410–22.
32. Wallace J and Kanaroglou P. The effect of temperature inversions on ground-level nitrogen dioxide (NO2) and fine particulate matter (PM2.5) using temperature profiles from the Atmospheric Infrared Sounder (AIRS). *Sci Total Environ* 2009; **407**: 5085–95.
33. Holzworth GC. Vertical temperature structure during the 1966 Thanksgiving week air pollution episode in New York city. *Mon Weather Rev* 1972; **100**: 445–50.
34. Janhäll S, Olofson KFG and Andersson PU *et al.* Evolution of the urban aerosol during winter temperature inversion episodes. *Atmos Environ* 2006; **40**: 5355–66.
35. Luo Y, Lu D and Zhou X *et al.* Characteristics of the spatial distribution and yearly variation of aerosol optical depth over China in last 30 years. *J Geophys Res* 2001; **106**: 14501–13.
36. Shi G, Hayasaka T and Ohmura A *et al.* Data quality assessment and the long-term trend of ground solar radiation in China. *J Appl Meteorol Climatol* 2008; **47**: 1006–16.
37. Guo JP, Zhang XY and Wu YR *et al.* Spatio-temporal variation trends of satellite-based aerosol optical depth in China during 1980–2008. *Atmos Environ* 2011; **45**: 6802–11.
38. Xin J, Wang Y and Li Z *et al.* Aerosol optical depth (AOD) and Ångström exponent of aerosols observed by the Chinese Sun Hazemeter Network from August 2004 to September 2005. *J Geophys Res* 2007; **112**: D05203.
39. Zhang XY, Wang YQ and Zhang XC *et al.* Carbonaceous aerosol composition over various regions of China during 2006. *J Geophys Res* 2008; **113**: D14111.
40. Guo JP, Zhang XY and Che HZ *et al.* Correlation between PM concentrations and aerosol optical depth in eastern China. *Atmos Environ* 2009; **43**: 5876–86.
41. Che H, Zhang XY and Xia X *et al.* Ground-based aerosol climatology of China: aerosol optical depths from the China Aerosol Remote Sensing Network (CARSNET) 2002–2013. *Atmos Chem Phys* 2015; **15**: 7619–52.
42. Xin JY, Wang YS and Pan YP *et al.* The campaign on atmospheric aerosol research network of China: CARE-China. *Bull Am Meteorol Soc* 2015; **96**: 1137–55.
43. Li Z, Chen H and Cribb M *et al.* Preface to special section on East Asian Studies of Tropospheric Aerosols: an International Regional Experiment (EAST-AIRE). *J Geophys Res* 2007; **112**: D22S00.
44. Li Z, Li C and Chen H *et al.* East Asian Studies of Tropospheric Aerosols and their Impact on Regional Climate (EAST-AIRC): an overview. *J Geophys Res Atmos* 2011; **116**: D00K34.
45. Lee KH, Li Z and Wong MS *et al.* Aerosol single scattering albedo estimated across China from a combination of ground and satellite measurements. *J Geophys Res* 2007; **112**: D22S15.
46. Liu J, Xie P and Wang Y *et al.* Haze observation and control measure evaluation in Jing-Jin-Ji (Beijing, Tianjin, Hebei) area during the period of the Asia-Pacific Economic Cooperation (APEC) Meeting. *Bull Chin Acad Sci* 2015; **30**: 368–77.
47. Huang RJ, Zhang Y and Bozzetti C *et al.* High secondary aerosol contribution to particulate pollution during haze events in China. *Nature* 2014; **514**: 218–22.
48. Sun YL, Jiang Q and Wang Z *et al.* Investigation of the sources and evolution processes of severe haze pollution in Beijing in January 2013. *J Geophys Res Atmos* 2014; **119**: 4380–98.
49. Guo S, Hu M and Zamora ML *et al.* Elucidating severe urban haze formation in China. *Proc Natl Acad Sci USA* 2014; **111**: 17373–8.

50. Zhang R, Wang G and Song G *et al.* Formation of urban fine particulate matter. *Chem Rev* 2015; **115**: 3803–55.
51. Yue DL, Hu M and Zhang R *et al.* the roles of sulfuric acid in new particle formation and growth in the mega-city of Beijing. *Atmos Chem Phys* 2010; **10**: 4953–60.
52. Yue DL, Hu M and Zhang R *et al.* Potential contribution of new particle formation to cloud condensation nuclei in Beijing. *Atmos Environ* 2011; **45**: 6070–7.
53. Zhang R, Suh I and Zhao J *et al.* Atmospheric new particle formation enhanced by organic acids. *Science* 2004; **304**: 1487–90.
54. Zhao J, Khalizov A and Zhang R *et al.* Hydrogen-bonding interaction in molecular complexes and clusters of aerosol nucleation precursors. *J Phys Chem A* 2009; **113**: 680–9.
55. Guo J, Xia F and Liu H *et al.* Impact of diurnal variability and meteorological factors on the PM2.5 - AOD relationship: implications for PM2.5 remote sensing. *Environ Pollut* 2017; **221**: 94–104.
56. Li C, Marufu LT and Dickerson RR *et al.* In situ measurements of trace gases and aerosol optical properties at a rural site in northern China during East Asian study of tropospheric aerosols: an international regional experiment 2005. *J Geophys Res Atmos* 2007; **112**: D22S04.
57. Zhang R, Li Q and Zhang R. Meteorological conditions for the persistent severe fog and haze event over eastern China in January 2013. *Sci China Earth Sci* 2014; **57**: 26–35.
58. Liu T, Gong S and He J *et al.* Attributions of meteorological and emission factors to the 2015 winter severe haze pollution episodes in China's Jing-Jin-Ji area. *Atmos Chem Phys* 2017; **17**: 2971–80.
59. Cai W, Li K and Liao H *et al.* Weather conditions conducive to Beijing severe haze more frequent under climate change. *Nat Clim Change* 2017; **7**: 257–62.
60. Zou Y, Wang Y and Zhang Y *et al.* Arctic sea ice, Eurasia snow, and extreme winter haze in China. *Sci Adv* 2017; **3**, e1602751.
61. Fu H and Chen J. Formation, features and controlling strategies of severe haze-fog pollutions in China. *Sci Total Environ* 2017; **578**: 121–38.
62. Li YJ, Sun Y and Zhang Q *et al.* Real-time chemical characterization of atmospheric particulate matter in China: a review. *Atmos Environ* 2017; **158**: 270–304.
63. Liao H and Seinfeld J. Radiative forcing by mineral dust aerosols: sensitivity to key variables. *J Geophys Res* 1998; **103**: 31637–45.
64. Liu P, Zhao C and Zhang Q *et al.* Aircraft study of aerosol vertical distributions over Beijing and their optical properties. *Tellus B* 2009; **61**: 756–67.
65. Zhang Q, Zhao C and Tie X *et al.* Characterizations of aerosols over the Beijing region: a case study of aircraft measurements. *Atmos Environ* 2006; **40**: 4513–27.
66. Zhang Q, Ma X and Tie X *et al.* Vertical distributions of aerosols under different weather conditions: analysis of in-situ aircraft measurements in Beijing, China. *Atmos Environ* 2009; **43**: 5526–35.
67. Winker DM, Hunt WH and McGill MJ. Initial performance assessment of CALIOP. *Geophys Res Lett* 2007; **34**: L19803..
68. Winker D, Pelon J and Coakley J, Jr *et al.* The CALIPSO mission: a global 3D view of aerosols and clouds. *Bull Am Meteorol Soc* 2010; **91**: 1211.
69. Huang J, Guo J and Wang F *et al.* CALIPSO inferred most probable heights of global dust and smoke layers. *J Geophys Res Atmos* 2015; **120**: 5085–100.
70. Terry D. A review of global stratospheric aerosol: measurements, importance, life cycle, and local stratospheric aerosol. *Atmos Res* 2008; **90**: 223–32.
71. Welton EJ, Voss KJ and Quinn PK *et al.* Measurements of aerosol vertical profiles and optical properties during INDOEX 1999 using micropulse lidars. *J Geophys Res* 2002; **107**: 8019.
72. Guo JP, Zhang XY and Cao CX *et al.* Monitoring haze episodes over the Yellow Sea by combining multisensor measurements. *Int J Rem Sens* 2010; **31**: 4743–55.
73. Campbell JR, Welton EJ and Spinhirne JD *et al.* Micropulse lidar observations of tropospheric aerosols over northeastern South Africa during the ARREX and SAFARI 2000 dry season experiments. *J Geophys Res* 2003; **108**: (D13).
74. Zhao D, Tie X and Gao Y *et al.* In-situ aircraft measurements of the vertical distribution of black carbon in the lower troposphere of Beijing, China, in the spring and summer time. *Atmosphere* 2015; **6**:713–31.
75. Adams AM, Prospero JM and Zhang C. CALIPSO -derived three-dimensional structure of aerosol over the Atlantic basin and adjacent continents. *J Clim* 2012; **25**: 6862–79.
76. Huang J, Minnis P and Yi Y *et al.* Summer dust aerosols detected from CALIPSO over the Tibetan Plateau. *Geophys Res Lett* 2007; **34**: 18.
77. Guo JP, Niu T and Wang F *et al.* Integration of multi-source measurements to monitor sand-dust storms over North China: a case study. *Acta Meteorol Sin* 2013; **27**: 566.
78. Guo JP, Liu H and Wang F *et al.* Three-dimensional structure of aerosol in China: a perspective from multi-satellite observations. *Atmos Res* 2016; **178–179**: 580–9.
79. Tian P, Cao X and Zhang L *et al.* Aerosol vertical distribution and optical properties over China from long-term satellite and ground-based remote sensing. *Atmos Chem Phys* 2017; **17**: 2509–23.
80. Ding G, Chan CY and Gao ZQ *et al.* Vertical structures of $PM_{10}$ and $Pm_{2.5}$ and their dynamical character in low atmosphere in Beijing urban areas. *Sci China Earth Sci* 2005; **48** Supp. II: 38–54.
81. Guinot B, Roger JC and Cachier H *et al.* Impact of vertical atmospheric structure on Beijing aerosol distribution. *Atmos Environ* 2006; **40**: 5167–80.
82. Meng ZY, Ding GA and Xu XB *et al.* Vertical distributions of $SO_2$ and $NO_2$ in the lower atmosphere in Beijing urban areas, China. *Sci Total Environ* 2008; **390**: 456–65.
83. Sun Y, Wang Y and Zhang C. Measurement of the vertical profile of atmospheric $SO_2$ during the heating period in Beijing on days of high air pollution. *Atmos Environ* 2009; **43**: 468–72.
84. Sun Y, Song T and Tang G *et al.* The vertical distribution of PM2.5 and boundary-layer structure during summer haze in Beijing, *Atmos Environ* 2013; **74**: 413–21.
85. Li X, An J and Wang Y *et al.* Studies on the measurement of atmospheric ozone in summer with Beijing meteorological tower. *China Environ Sci* 2003; **23**: 353–7.
86. Sun YL, Du W and Wang Q *et al.* Real-time characterization of aerosol particle composition above the urban canopy in Beijing: insights into the interactions between the atmospheric boundary layer and aerosol chemistry. *Environ Sci Technol* 2015; **49**: 11340–7.
87. Sun YL, Wang Z and Wild O *et al.* "APEC Blue": secondary aerosol reductions from emission controls in Beijing. *Sci Rep* 2016; **6**: 20668.
88. Xue L, Ding A and Gao J *et al.* Aircraft measurements of the vertical distribution of sulfur dioxide and aerosol scattering coefficient in China. *Atmos Environ* 2010; **44**: 278–82.
89. Liu J, Zheng Y and Li Z *et al.* Seasonal variations of aerosol optical properties, vertical distribution and associated radiative effects in the Yangtze Delta region of China. *J Geophys Res Atmos* 2012; **117**: D00K38.

90. Li J, Fu Q and Huo J *et al.* Tethered balloon-based black carbon profiles within the lower troposphere of Shanghai in the 2013 East China smog. *Atmos Environ* 2015; **123**: 327–38.
91. Wang R, Xu X and Jia S *et al.* Lower tropospheric distributions of $O_3$ and aerosol over Raoyang, a rural site in the North China Plain. *Atmos Chem Phys* 2017; **17**: 3891–903.
92. Baklanov AA, Grisogono B and Bornstein R *et al.* The nature, theory, and modeling of atmospheric planetary boundary layers. *Bull Am Meteorol Soc* 2011; **92**: 123–8.
93. Boutle IA, Beare RJ and Belcher SE *et al.* The moist boundary layer under a mid-latitude weather system. *Bound Layer Meteorol* 2010; **134**: 367–86.
94. Cuxart J, Yagüe C and Morales G *et al.* Stable atmospheric boundary-layer experiment in Spain (SABLES 98): a report. *Bound Layer Meteorol* 2000; **96**: 337–70.
95. Poulos GS, Blumen W and Fritts DC *et al.* CASES-99: a comprehensive investigation of the stable nocturnal boundary layer. *Bull Am Meteorol Soc* 2002; **83**: 555–81.
96. Grachev AA, Andreas EL and Fairall CW *et al.* Turbulent measurements in the stable atmospheric boundary layer during SHEBA: ten years after. *Acta Geophys* 2008; **56**: 142–66.
97. Mahrt L. Stratified atmospheric boundary layers. *Bound-Layer Meteorol* 1999; **90**: 375–96.
98. Shraiman BI and Siggia ED. Scalar turbulence. *Nature* 2000; **405**: 639–46.
99. Huang NE, Shen Z and Long SR *et al.* The empirical mode decomposition and the Hilbert spectrum for nonlinear and non-stationary time series analysis. *Proc Math Phys Eng Sci* 1998; **454A**: 903–95.
100. Huang YX, Schmitt FG and Gagne Y *et al.* Application of arbitrary-order Hilbert spectral analysis to passive scalar turbulence. *J Phys: Conf Ser* 2011; **318**: 042003.
101. Wei W, Zhang HS and Schmitt FG *et al.* Investigation of turbulence behaviour in the stable boundary layer using arbitrary-order Hilbert spectra. *Bound Layer Meteorol* 2017; **163**: 311–26.
102. Vautard R, Moran MD and Solazzo E *et al.* Evaluation of the meteorological forcing used for the air quality model evaluation international initiative (aqmeii) air quality simulations. *Atmos Environ* 2012; **53**: 15–37.
103. Zhang H, Pu Z and Zhang X. Examination of errors in near-surface temperature and wind from wrf numerical simulations in regions of complex terrain. *Weather Forecast* 2013; **28**: 893–914.
104. Seibert P. Review and intercomparison of operational methods for the determination of the mixing height. *Atmos Environ* 2000; **34**: 1001–27.
105. Durre I and Yin X. Enhanced radiosonde data for studies of vertical structure. *Bull Am Meteorol Soc* 2008; **89**: 1257–62.
106. Liu S and Liang XZ. Observed diurnal cycle climatology of planetary boundary layer height. *J Clim* 2010; **23**: 5790–809.
107. Seidel DJ, Ao CO and Li K. Estimating climatological planetary boundary layer heights from radiosonde observations: Comparison of methods and uncertainty analysis. *J Geophys Res* 2010; **115**: D16.
108. Guo JP, Miao Y and Zhang Y *et al.* The climatology of planetary boundary layer height in China derived from radiosonde and reanalysis data. *Atmos Chem Phys* 2016; **16**: 13309–19.
109. Gupta P and Christopher SA. Particulate matter air quality assessment using integrated surface, satellite, and meteorological products: multiple regression approach. J Geophys Res Atmos 2009; **114**: D14205..
110. Liu Y, Paciorek CJ and Koutrakis P. Estimating regional spatial and temporal variability of PM2.5 concentrations using satellite data, meteorology, and land use information. *Environ Health Perspect* 2009; **117**:886–92.
111. Wu YR, Guo JP and Zhang XY *et al.* Synergy of satellite and ground based observations in estimation of particulate matter in eastern China. *Sci Total Environ* 2012; **433**: 20–30.
112. Davis KJ, Gamage N and Hagelberg CR *et al.* An objective method for deriving atmospheric structure from airborne lidar observations. *J Atmos Ocean Tech* 2000; **17**: 1455–68.
113. Brooks IM. Finding boundary layer top: application of a wavelet covariance transform to lidar backscatter profiles. *J Atmos Ocean Tech* 2003; **20**: 1092–105.
114. Steyn DG, Baldi M and Hoff RM. The detection of mixed layer depth and entrainment zone thickness from lidar backscatter profiles. *J Atmos Ocean Tech* 1999; **16**: 953–9.
115. Press WH, Teukolsky SA and Vetterling WT *et al. Numerical Recipes in C: The Art of Scientific Computing*. 2nd edn. Cambridge: Cambridge University Press, 1992.
116. Sawyer V and Li Z. Detection, variations and intercomparison of the planetary boundary layer depth from radiosonde, lidar and infrared spectrometer. *Atmos Environ* 2013; **79**: 518–28.
117. Han S, Bian H and Tie X *et al.* Impact of nocturnal planetary boundary layer on urban air pollutants: measurements from a 250-m tower over Tianjin, China. *J Hazard Mater* 2009; **162**: 264–9.
118. Miao S, Dou J and Chen F *et al.* Analysis of observations on the urban surface energy balance in Beijing. *Sci China Earth Sci* 2012; **55**: 1881–90.
119. Beyrich F. Mixing height estimation from sodar data — a critical discussion. *Atmos Environ* 1997; **31**: 3941–53.
120. Yang K, Koike T and Fujii H *et al.* The daytime evolution of the atmospheric boundary layer and convection over the Tibetan Plateau: observations and simulations. *J Meteorol Soc Japan* 2004; **82**: 1777–92.
121. May PT and Wilczak JM. Diurnal and seasonal variations of boundary-layer structure observed with a radar wind profiler and RASS. *Mon Weather Rev* 1993; **121**: 673–82.
122. Mitchell MJ, Arritt RW and Labas K. A climatology of the warm season Great Plains low-level jet using wind profiler observations. *Weather Forecast* 1995; **10**: 576–91.
123. Lundquist JK, Wliczak JM and Ashton R *et al.* Assessing state-of-the-art capabilities for probing the atmospheric boundary layer: the XPIA field campaign. *Bull Am Meteorol Soc* 2016; **98**: 289–314.
124. Du Y, Zhang Q and Ying Y *et al.* Characteristics of low-level jets in Shanghai during the 2008-2009 warm seasons as inferred from wind profiler radar data. *J Meteorol Soc Japan* 2012; **90**: 891–903.
125. Wei W, Zhang HS and Ye XX. Comparison of low-level jets along the north coast of China in summer. *J Geophys Res Atmos* 2014; **119**: 9692–706.
126. Cohn SA and Angevine WM. Boundary layer height and entrainment zone thickness measured by lidars and wind-profiling radars. *J Appl Meteorol* 2000; **39**: 1233–47.
127. White AB, Senff CJ and Banta RM. A comparison of mixing depths observed by ground-based wind profilers and an airborne lidar. *J Atmos Ocean Tech* 1999; **16**: 584–90.
128. Liu J, Huang J and Chen B *et al.* Comparisons of PBL heights derived from CALIPSO and ECMWF reanalysis data over China. *J Quant Spectrosc Radiat Transfer* 2015; **153**: 102–12.
129. Zhang W, Guo J and Miao Y *et al.* Planetary boundary layer height from CALIOP compared to radiosonde over China. *Atmos Chem Phys* 2016; **16**: 9951–63.
130. Ho SP, Peng L and Anthes RA *et al.* Marine boundary layer heights and their longitudinal, diurnal, and interseasonal variability in the Southeastern Pacific using COSMIC, CALIOP, and radiosonde data. *J Clim* 2015; **28**: 2856–72.

131. Leventidou E, Zanis P and Balis D *et al.* Factors affecting the comparisons of planetary boundary layer height retrievals from CALIPSO, ECMWF and radiosondes over Thessaloniki, Greece. *Atmos Environ* 2013; **74**: 360–6.
132. Campbell JR, Hlavka DL and Welton EJ *et al.* Full-time, eye-safe cloud and aerosol lidar observation at atmospheric radiation measurement program sites: instruments and data processing. *J Atmos Ocean Tech* 2002; **19**: 431–42.
133. Spinhirne JD. Micro pulse lidar. *IEEE Trans Geosci Rem Sens* 1993; **31**: 48–55.
134. Welton EJ, Voss K and Gordon H *et al.* Ground-based lidar measurements of aerosols during ACE-2: instrument description, results, and comparisons with other ground-based and airborne measurements. *Tellus B* 2000; **52**: 635–50.
135. Niu F, Li Z and Li C *et al.* Increase of wintertime fog in China: potential impacts of weakening of the Eastern Asian monsoon circulation and increasing aerosol loading. *J Geophys Res* 2010; **115**: D00K20.
136. Xu M, Chang CP and Fu C *et al.* Steady decline of east Asian monsoon winds, 1969–2000: evidence from direct ground measurements of wind speed. *J Geophys Res* 2006; **111**: D24111.
137. Yang X, Yao Z and Li Z *et al.* Heavy air pollution suppresses summer thunderstorms in central China. *J Atmos Sol Terr Phys* 2013; **95–96**: 28–40.
138. Yang X, Ferrat M and Li Z. New evidence of orographic precipitation suppression by aerosols in central China. *Meteorol Atmos Phys* 2013; **119**: 17–29.
139. Jacobson MZ and Kaufman YJ. Wind reduction by aerosol particles. *Geophys Res Lett*, 2006; **33**: 17.
140. Yang X and Li Z. Increases in thunderstorm activity and relationships with air pollution in southeast China. *J Geophys Res Atmos* 2014; **119**: 1835–44.
141. Zhang R, Khalizov AF and Pagels J *et al.* Variability in morphology, hygroscopicity, and optical properties of soot aerosols during atmospheric processing. *Proc Natl Acad Sci USA* 2008; **105**: 10291–6.
142. Khalizov AF, Zhang R and Zhang D *et al.* Formation of highly hygroscopic soot aerosols upon internal mixing with sulfuric acid vapor. *J Geophys Res* 2009; **114**: D05208.
143. Khalizov AF, Xue H and Wang L *et al.* Enhanced light absorption and scattering by carbon soot aerosol internally mixed with sulfuric acid. *J Phys Chem A* 2009; **113**: 1066–74.
144. Ding A, Nie WX and Huang X *et al.* Long-term observation of air pollution-weather/climate interactions at the SORPES station: a review and outlook. *Front Environ Sci Eng* 2016; **10**: 15.
145. Dong Z, Li Z and Yu X *et al.* Opposite long-term trends in aerosols between lower and higher altitudes: a testimony to the aerosol-PBL feedback. *Atmos Chem Phys*, 2017; **17**: 7997–8009.
146. Ran L, Deng Z and Xu X *et al.* Vertical profiles of black carbon measured by a micro-aethalometer in summer in the North China Plain. *Atmos Chem Phys* 2016; **16**: 10441–54.
147. Ding AJ, Wang T and Thouret V *et al.* Tropospheric ozone climatology over Beijing: analysis of aircraft data from the MOZAIC program. *Atmos Chem Phys* 2008; **8**: 1–13.
148. Gu Y, Liou KN and Mechoso CR *et al.* Climatic effects of different aerosol types in China simulated by the UCLA general circulation model. *J Geophys Res* 2006; **111**: D15201.
149. Donner LJ and Phillips VT. Boundary layer control on convective available potential energy: Implications for cumulus parameterization. *J Geophys Res* 2003; **108**: doi: 10.1029/2003JD003773.
150. Zhou X and Geerts B. The influence of soil moisture on the planetary boundary layer and on cumulus convection over an isolated mountain. Part I: observations. *Mon Weather Rev* 2013; **141**: 1061–78.
151. Medeiros B, Hall A and Stevens B. What controls the mean depth of the PBL? *J Clim* 2005; **18**: 3157–72.
152. Li Z, Niu F and Fan J *et al.* Long-term impacts of aerosols on the vertical development of clouds and precipitation. *Nat Geosci* 2011; **4**: 888–94.
153. Tao WK, Chen JP and Li Z *et al.* Impact of aerosols on convective clouds and precipitation. *Rev Geophys* 2012; **50**: doi:10.1029/2011RG000369.
154. Wang Y, Lee KH and Lin Y *et al.* Distinct effects of anthropogenic aerosols on tropical cyclones. *Nat Clim Change* 2014; **4**: 368–73.
155. Fan J, Rosenfeld D and Yang Y *et al.* Substantial contribution of anthropogenic air pollution to catastrophic floods in Southwest China. *Geophys Res Lett* 2015; **42**: 6066–75.
156. Lin Y, Wang Y and Pan B *et al.* Distinct impacts of aerosols on an evolving continental cloud complex during the RACORO field campaign. *J Atmos Sci* 2016; **73**: 3681–700.
157. Zhu B, Kang H and Zhu T *et al.* Impact of Shanghai urban land surface forcing on downstream city ozone chemistry. *J Geophys Res Atmos* 2015; **120**: 4340–51.
158. Kulmala M. Atmospheric science: how particles nucleate and grow. *Science* 2003; **302**: 1000–1.
159. Zhang R. Getting to the critical nucleus of aerosol formation. *Science* 2010; **328**: 1366–7.
160. Deng XJ, Zhou XJ and Tie XX *et al.* Attenuation of ultraviolet radiation reaching the surface due to atmospheric aerosols in Guangzhou. *Chin Sci Bull* 2012; **57**: 2759–66.
161. Mok J, Krotkov NA and Arola A *et al.* Impacts of brown carbon from biomass burning on surface UV and ozone photochemistry in the Amazon Basin. *Sci Rep* 2016; **6**: 36940.
162. Dickerson RR, Kondragunta S and Stenchikov G *et al.* The impact of aerosols on solar ultraviolet radiation and photochemical smog. *Science* 1997; **278**: 827–30.
163. Tao JC, Zhao CS and Ma N *et al.* The impact of aerosol hygroscopic growth on the single-scattering albedo and its application on the $NO_2$ photolysis rate coefficient. *Atmos Chem Phys* 2014; **14**:12055–67.
164. Meng Z, Dabdub D and Seinfeld JH. Chemical coupling between atmospheric ozone and particulate matter. *Science* 1997; **277**: 116–9.
165. Nishanth T, Praseed KM and Kumar MKS *et al.* Influence of ozone precursors and $PM_{10}$ on the variation of surface O3 over Kannur, India. *Atmos Res* 2014; **138**: 112–24.
166. Wang S. Study of atmospheric particulate-cloud-radiation-photochemical process on ozone in Nanjing. *Ph.D. Thesis*. Nanjing University 2014.
167. Tie X, Brasseur G and Emmons L *et al.* Effects of aerosols on tropospheric oxidants: a global model study. *J Geophys Res* 2001; **106**: 22931–64.
168. Tie X, Madronich S and Walters S *et al.* Assessment of the global impact of aerosols on tropospheric oxidants. *J Geophys Res* 2005; **110**: D03204.
169. Li J, Wang Z and Wang X *et al.* Impacts of aerosols on summertime tropospheric photolysis frequencies and photochemistry over Central Eastern China. *Atmos Environ* 2011; **45**: 1817–29.
170. Li G, Bei N and Tie X *et al.* Aerosol effects on the photochemistry in Mexico City during MCMA-2006/MILAGRO campaign. *Atmos Chem Phys* 2011; **11**: 5169–82.
171. Cai YF, Wang TJ and Xie M *et al.* Impacts of atmospheric particles on surface ozone in Nanjing. *Climatic Environ Res* 2013; **18**: 251–60.
172. Ravishankara AR. Heterogeneous and multiphase chemistry in the troposphere. *Science* 1997; **276**: 1058–65.
173. Jacob D. Heterogeneous chemistry and tropospheric ozone. *Atmos Environ* 2000; **34**: 2131–59.

174. Remorov RG, Gershenzon YM and Molina LT *et al.* Kinetics and mechanism of HO2 uptake on solid NaCl. *J Phys Chem A* 2002; **106**: 4558–65.
175. Hoffman RC, Kaleuati MA and Finlayson-Pitts BJ. Knudsen cell studies of the reaction of gaseous HNO3 with NaCl using less than a single layer of particles at 298 K: a modified mechanism. *J Phys Chem A* 2003; **107**: 7818–26.
176. Bauer SE, Balkanski Y and Schulz M *et al.* Global modeling of heterogeneous chemistry on mineral aerosol surfaces: Influence on tropospheric ozone chemistry and comparison to observations. *J Geophys Res* 2004; **109**: D02304.
177. McNaughton CS, Clarke AD and Kapustin V *et al.* Observations of heterogeneous reactions between Asian pollution and mineral dust over the Eastern North Pacific during INTEX-B. *Atmos Chem Phys* 2009; **9**: 8283–308.
178. Kleffmann J and Wiesen P. Heterogeneous conversion of NO2 and NO on HNO3 treated soot surfaces: atmospheric implications. *Atmos Chem Phys* 2005; **5**: 77–83.
179. Kaiser JC, Riemer N and Knopf DA. Detailed heterogeneous oxidation of soot surfaces in a particle-resolved aerosol model. *Atmos Chem Phys* 2011; **11**: 4505–20.
180. Liao H and Seinfeld JH. Global impacts of gas-phase chemistry-aerosol interactions on direct radiative forcing by anthropogenic aerosols and ozone. *J Geophys Res* 2005; **110**: D18208.
181. Deng J, Wang T and Liu L *et al.* Modeling heterogeneous chemical processes on aerosol surface. *Particuology* 2010; **8**: 308–18.
182. Lou S, Liao H and Zhu B. Impacts of aerosols on surface-layer ozone concentrations in China through heterogeneous reactions and changes in photolysis rates. *Atmos Environ* 2014; **85**: 123–38.
183. Zhang R, Leu MT and Keyser LF. Hydrolysis of $N_2O_5$ and $ClONO_2$ on the $H_2SO_4/HNO_3/H_2O$ ternary solutions under stratospheric conditions. *Geophys Res Lett* 1995; **22**: 1493–6.
184. Zhao J, Levitt NP and Zhang R *et al.* Heterogeneous reactions of methylglyoxal in acidic media: implications for secondary organic aerosol formation. *Environ Sci Technol* 2006; **40**: 7682–7.
185. Qiu C and Zhang R. Multiphase chemistry of atmospheric amines. *Phys Chem Chem Phys* 2013; **15**: 5738–52.
186. Zhang DL, Shou YX and Dickerson R *et al.* Impact of upstream urbanization on the urban heat island effects along the Washington–Baltimore corridor. *J Appl Meteorol Climatol* 2011; **50**: 2012–29.
187. Xie M, Liao J and Wang T *et al.* Modeling of the anthropogenic heat flux and its effect on regional meteorology and air quality over the Yangtze River Delta region, China. *Atmos Chem Phys* 2016; **16**: 6071–89.
188. Cao C, Lee X and Liu S *et al.* Urban heat islands in China enhanced by haze pollution. *Nat Comm* 2016; **7**: 12509.
189. Aan de Brugh JMJ, Ouwersloot HG and Vilà-Guerau de Arellano J *et al.* A large-eddy simulation of the phase transition of ammonium nitrate in a convective boundary layer. *J Geophys Res Atmos* 2013; **118**: 826–36.
190. Barbaro E, Krol M and Vilà-Guerau de Arellano J. Numerical simulation of the interaction between ammonium nitrate aerosol and convective boundary-layer dynamics. *Atmos Environ* 2015; **105**: 202–11.
191. Stevens B, Cotton WR and Feingold G *et al.* Large-eddy simulations of strongly precipitating, shallow, stratocumulus-topped boundary layers. *J Atmos Sci* 1998; **55**: 3616–38.
192. Jiang H, Feingold G and Cotton W. Simulations of aerosol-cloud-dynamical feedbacks resulting from entrainment of aerosol into the marine boundary layer during the Atlantic Stratocumulus Transition Experiment. *J Geophys Res* 2002; **107**: doi:10.1029/2001JD001502.
193. Ackerman AS, Kirkpatrick MP and Stevens DE *et al.* The impact of humidity above stratiform clouds on indirect aerosol climate forcing. *Nature* 2004; **432**: 1014–7.
194. Xu X and Xue H. Impacts of free-tropospheric temperature and humidity on nocturnal nonprecipitating marine stratocumulus. *J Atmos Sci* 2015; **72**: 2853–64.
195. Stevens B. On the growth of layers of nonprecipitating cumulus convection. *J Atmos Sci* 2007; **64**: 2916–31.
196. Xue H and Feingold G. Large-eddy simulations of trade wind cumuli: investigation of aerosol indirect effects. *J Atmos Sci* 2006; **63**: 1605–22.
197. Grabowski W, Wang LP and Prabha T. Macroscopic impacts of cloud and precipitation processes on maritime shallow convection as simulated by a large eddy simulation model with bin microphysics. *Atmos Chem Phys* 2015; **15**: 913–26.
198. Seifert A and Heus T. Large-eddy simulation of organized precipitating trade wind cumulus clouds. *Atmos Chem Phys* 2013; **13**: 5631–45.
199. Xue H, Feingold G and Stevens B. Aerosol effects on clouds, precipitation, and the organization of shallow cumulus convection. *J Atmos Sci* 2008; **65**: 392–406.
200. Feingold G, Koren I and Wang H *et al.* Precipitation-generated oscillations in open cellular cloud fields. *Nature* 2011; **466**: 849–52.
201. Chen G, Xue H and Feingold G *et al.* Vertical transport of pollutants by shallow cumuli from large eddy simulations. *Atmos Chem Phys* 2012; **12**: 11319–27.
202. Dorling SR, Davies TD and Pierce CE. Cluster analysis: a technique for estimating the synoptic meteorological controls on air and precipitation chemistry—method and applications. *Atmos Environ.* Part A. General Topics 1992; **26**: 2575–81.
203. Kallos G, Kassomenos P and Pielke RA. Synoptic and mesoscale weather conditions during air pollution episodes in Athens, Greece. *Bound Layer Meteorol* 1993; **62**: 163–84.
204. Nilsson ED, Paatero J and Boy M. Effects of air masses and synoptic weather on aerosol formation in the continental boundary layer. *Tellus B* 2001; **53**: 462–78.
205. Ding AJ, Wang T and Zhao M *et al.* Simulation of sea-land breezes and a discussion of their implications on the transport of air pollution during a multi-day ozone episode in the Pearl River Delta of China. *Atmos Environ* 2004; **38–39**: 6737–50.
206. Ding AJ, Wang T and Xue LK *et al.* Transport of north China air pollution by midlatitude cyclones: Case study of aircraft measurements in summer 2007. *J Geophys Res* 2009; **114**: D08304.
207. Zhang Y, Ding A and Mao H *et al.* Impact of synoptic weather patterns and inter-decadal climate variability on air quality in the North China Plain during 1980–2013. *Atmos Environ* 2016; **124**:119–28.
208. Binkowski FS and Roselle SJ. Models-3 Community Multiscale Air Quality (CMAQ) model aerosol component 1. model description. *J Geophys Res* 2003; **108**: doi:10.1029/2001JD001490.
209. Byun D and Schere KL. Review of the governing equations, computational algorithms, and other components of the Models-3 Community Multiscale Air Quality (CMAQ) modeling system. *Appl Mech Rev* 2006; **59**: 51–77.
210. Zhang MG, Uno I and Carmichael GR *et al.* Large-scale structure of trace gas and aerosol distributions over the western Pacific Ocean during the Transport and Chemical Evolution over the Pacific (TRACE-P) experiment. *J Geophys Res* 2003; **108**: 8820.
211. Streets DG, Fu JS and Jang CJ *et al.* Air quality during the 2008 Beijing Olympic Games. *Atmos Environ* 2007; **41**: 480–92.
212. Liu XH, Zhang Y and Cheng SH *et al.* Understanding of regional air pollution over China using CMAQ, part I performance evaluation and seasonal variation. *Atmos Environ* 2010; **44**: 2415–26.

213. Wang SX, Zhao M and Xing J *et al.* Quantifying the air pollutants emission reduction during the 2008 Olympic Games in Beijing. *Environ Sci Technol* 2010; **44**: 2490–6.
214. Wang LT, Wei Z and Yang J *et al.* The 2013 severe haze over southern Hebei, China: model evaluation, source apportionment, and policy implications. *Atmos Chem Phys* 2014; **14**: 3151–73.
215. Wang Z, Li J and Wang Z *et al.* Modeling study of regional severe hazes over mid-eastern China in January 2013 and its implications on pollution prevention and control. *Sci China Earth Sci* 2014; **57**: 3–13.
216. Wang J, Wang S and Jiang J *et al.* Impact of aerosol–meteorology interactions on fine particle pollution during China's severe haze episode in January 2013. *Environ Res Lett* 2014; **9**: 094002.
217. Wang H, Shi GY and Zhang XY *et al.* Mesoscale modelling study of the interactions between aerosols and PBL meteorology during a haze episode in China Jing–Jin–Ji and its near surrounding region – part 2: aerosols' radiative feedback effects. *Atmos Chem Phys* 2015; **15**: 3277–87.
218. Huang X, Ding A and Liu L *et al.* Effects of aerosol–radiation interaction on precipitation during biomass-burning season in East China. *Atmos Chem Phys* 2016; **16**: 10063–82.
219. Liu L, Huang X and Ding A *et al.* Dust-induced radiative feedbacks in north China: a dust storm episode modeling study using WRF-Chem. *Atmos Environ* 2016; **129**: 43–54.
220. Dawson JP, Adams PJ and Pandis SN. Sensitivity of PM2.5 to climate in the Eastern US: a modeling case study. *Atmos Chem Phys* 2007; **7**: 4295–309.
221. Liao H, Zhang Y and Chen WT *et al.* Effect of chemistry-aerosol-climate coupling on predictions of future climate and future levels of tropospheric ozone and aerosols. *J Geophys Res* 2009; **114**: D10306.
222. Von Schneidemesser E, Monks PS and Allan JD *et al.* Chemistry and the linkages between air quality and climate change. *Chem Rev* 2015; **1**: 3856–97.
223. Jacob DJ and Winner DA. Effect of climate change on air quality. *Atmos Environ* 2009; **43**: 51–63.
224. Fang Y, Fiore AM and Horowitz LW *et al.* The impacts of changing transport and precipitation on pollutant distributions in a future climate. *J Geophys Res Atmos* 2011; **116**: 1–14.
225. Allen RJ, Landuyt W and Rumbold ST. An increase in aerosol burden and radiative effects in a warmer world. *Nat Clim Change* 2015; **6**: 269–74.
226. Zhang L, Liao H and Li J. Impacts of Asian summer monsoon on seasonal and interannual variations of aerosols over eastern China. *J Geophys Res Atmos* 2010; **115**: D00K05.
227. Zhu J, Liao H and Li J. Increases in aerosol concentrations over eastern China due to the decadal-scale weakening of the East Asian summer monsoon. *Geophys Res Lett* 2012; **39**: L09809.
228. Mu Q and Liao H. Simulation of the interannual variations of aerosols in China: role of variations in meteorological parameters. *Atmos Chem Phys* 2014; **14**: 9597–612.
229. Yang Y, Liao H and Lou S. Decadal trend and interannual variation of outflow of aerosols from East Asia: roles of variations in meteorological parameters and emissions. *Atmos Environ* 2015; **100**: 141–53.
230. Feng J, Liao H and Gu Y. A comparison of meteorology-driven interannual variations of surface aerosol concentrations in the eastern United States, eastern China, and Europe. *Sci Online Lett Atmos* 2016; **12**: 146–52.
231. Yang YQ, Wang JZ and Gong SL *et al.* PLAM - a meteorological pollution index for air quality and its applications in fog-haze forecasts in North China. *Atmos Chem Phys* 2016; **16**: 1353–64.
232. Fu Y, Tai APK and Liao H. Impacts of historical climate and land cover changes on fine particulate matter (PM2.5) air quality in East Asia between 1980 and 2010. *Atmos Chem Phys* 2016; **16**:10369–83.
233. Wang HJ, Chen H and Liu J. Arctic sea ice decline intensified haze pollution in eastern China. *Atmos Ocean Sci Lett* 2015; **8**: 1–9.
234. Yang Y, Russell LM and Lou S *et al.* Dust-wind interactions can intensify aerosol pollution over eastern China. *Nat Comm* 2017; **8**: 15333.
235. Zhao S, Li J and Sun C. Decadal variability in the occurrence of wintertime haze in central eastern China tied to the Pacific Decadal Oscillation. *Sci Rep* 2016; **6**: 27424.
236. Oshima N, Kondo Y and Moteki N *et al.* Wet removal of black carbon in Asian outflow: Aerosol Radiative Forcing in East Asia (A-FORCE) aircraft campaign. *J Geophys Res* 2012; **117**: D03204.
237. Park S and Allen RJ. Understanding influences of convective transport and removal processes on aerosol vertical distribution. *Geophys Res Lett* 2015; **42**: 10438–44.
238. Stull RB (ed). *An Introduction to Boundary Layer Meteorology*. Dordrecht: Springer, 1988.
239. Matthias V, Balis D and Bösenberg J *et al.* Vertical aerosol distribution over Europe: statistical analysis of Raman lidar data from 10 European Aerosol Research Lidar Network (EARLINET) stations. *J Geophys Res* 2004; **109**: 1–12.
240. Miao Y, Guo J and Liu S *et al.* Classification of summertime synoptic patterns in Beijing and their associations with boundary layer structure affecting aerosol pollution. *Atmos Chem Phys* 2017; **17**: 3097–110.
241. Miao Y, Hu XM and Liu S *et al.* Seasonal variation of local atmospheric circulations and boundary layer structure in the Beijing-Tianjin-Hebei region and implications for air quality. *J Adv Model Earth Syst* 2015; **7**: 1602–26.
242. Quan J, Gao Y and Zhang Q *et al.* Evolution of planetary boundary layer under different weather conditions, and its impact on aerosol concentrations. *Particuology* 2013; **11**: 34–40.
243. Garratt J. Review: the atmospheric boundary layer. *Earth Sci Rev* 1994; **37**: 89–134.
244. Yi C, Davis KJ and Berger BW *et al.* Long-term observations of the dynamics of the continental planetary boundary layer. *J Atmos Sci* 2001; **58**: 1288–99.
245. Maletto A, McKendry IG and Strawbridge KB. Profiles of particulate matter size distributions using a balloon-borne lightweight aerosol spectrometer in the planetary boundary layer. *Atmos Environ* 2003; **37**: 661–70.
246. Chen Y, Zhao C and Zhang Q *et al.* Aircraft study of mountain chimney effect of Beijing, China. *J Geophys Res* 2009; **114**: 1–10.
247. Liu S, Liu Z and Li J *et al.* Numerical simulation for the coupling effect of local atmospheric circulations over the area of Beijing, Tianjin and Hebei Province. *Sci China Earth Sci* 2009; **52**: 382–92.
248. Hu XM, Ma Z and Lin W *et al.* Impact of the Loess Plateau on the atmospheric boundary layer structure and air quality in the North China Plain: a case study. *Sci Total Environ* 2014; **499**: 228–37.
249. De Wekker SFJ. Observational and numerical evidence of depressed convective boundary layer heights near a mountain base. *J Appl Meteorol Climatol* 2008; **47**:1017–26.
250. Lu R and Turco RP. Air pollutant transport in a coastal environment—II. Three-dimensional simulations over Los Angeles basin. *Atmos Environ* 1995; **29**: 1499–518.
251. Miao Y, Liu S and Zheng Y *et al.* Numerical study of the effects of local atmospheric circulations on a pollution event over Beijing–Tianjin–Hebei, China. *J Environ Sci* 2015; **30**: 9–20.
252. Miller STK. Sea breeze: structure, forecasting, and impacts. *Rev Geophys* 2003; **41**: 1011.
253. Lo JCF, Lau AKH and Fung J *et al.* Investigation of enhanced cross-city transport and trapping of air pollutants by coastal and urban land-sea breeze circulations. *J Geophys Res* 2006; **111**: 1–13.